

Colloquium: Mechanical formalisms for tissue dynamics

Sham Tlili¹, Cyprien Gay^{1,6,a}, François Graner^{1,6,b}, Philippe Marcq², François Molino^{3,4,6}, and Pierre Saramito^{5,6}

¹ Laboratoire Matière et Systèmes Complexes, Université Denis Diderot - Paris 7, CNRS UMR 7057, 10 rue Alice Domon et Léonie Duquet, F-75205 Paris Cedex 13, France

² Laboratoire Physico-Chimie Curie, Institut Curie, Université Marie et Pierre Curie - Paris 6, CNRS UMR 168, 26 rue d'Ulm, F-75248 Paris Cedex 05, France

³ Laboratoire Charles Coulomb, Univ. Montpellier II, CNRS UMR 5221, Place Eugène Bataillon, CC070, F-34095 Montpellier Cedex 5, France

⁴ Institut de Génomique Fonctionnelle, Univ. Montpellier I, Univ. Montpellier II, 141 rue de la Cardonille, CNRS UMR 5203, INSERM UMR.S 661, F-34094 Montpellier Cedex 05, France

⁵ Laboratoire Jean Kuntzmann, Université Joseph Fourier - Grenoble I, CNRS UMR 5524, BP 53, F-38041 Grenoble Cedex, France

⁶ Academy of Bradylogists - Paris Cedex 13, France

Received 27 September 2013 and Received in final form 22 December 2014

Published online: 13 May 2015 – © EDP Sciences / Società Italiana di Fisica / Springer-Verlag 2015

Abstract. The understanding of morphogenesis in living organisms has been renewed by tremendous progress in experimental techniques that provide access to cell scale, quantitative information both on the shapes of cells within tissues and on the genes being expressed. This information suggests that our understanding of the respective contributions of gene expression and mechanics, and of their crucial entanglement, will soon leap forward. Biomechanics increasingly benefits from models, which assist the design and interpretation of experiments, point out the main ingredients and assumptions, and ultimately lead to predictions. The newly accessible local information thus calls for a reflection on how to select suitable classes of mechanical models. We review both mechanical ingredients suggested by the current knowledge of tissue behaviour, and modelling methods that can help generate a rheological diagram or a constitutive equation. We distinguish cell scale (“intra-cell”) and tissue scale (“inter-cell”) contributions. We recall the mathematical framework developed for continuum materials and explain how to transform a constitutive equation into a set of partial differential equations amenable to numerical resolution. We show that when plastic behaviour is relevant, the dissipation function formalism appears appropriate to generate constitutive equations; its variational nature facilitates numerical implementation, and we discuss adaptations needed in the case of large deformations. The present article gathers theoretical methods that can readily enhance the significance of the data to be extracted from recent or future high throughput biomechanical experiments.

1 Introduction

1.1 Motivations

While biologists use the word “model” for an organism studied as an archetype, such as *Drosophila* or *Arabidopsis*, physicists rather use this word for models based on either analytical equations or numerical simulations. Biomechanical models have a century-old tradition and play several roles [1]. For instance, they assist experiments to integrate and manipulate quantitative data, and extract measurements of relevant parameters (either directly, or

through fits of models to data). They also lead to predictions, help to propose and design new experiments, test the effect of parameters, simulate several realisations of a stochastic phenomenon, or simulate experiments which cannot be implemented in practice. They enable to illustrate an experiment, favor its interpretation and understanding. They point out the main ingredients and assumptions, test the sensitivity of an experiment to a parameter or to errors, and determine which assumptions are sufficient to describe an experimental result. Models can help to determine whether two facts which appear similar have a superficial or deep analogy, and whether two facts which are correlated are causally related or not.

Two themes have dominated the recent literature: modelling the mechanics of some specific adult tissues like

^a e-mail: cyprien.gay@univ-paris-diderot.fr

^b e-mail: francois.graner@univ-paris-diderot.fr

bones or muscles, for which deformations and stresses are obviously part of the biological function [2, 3]; and unraveling the role of forces in the generation of forms during embryonic development [4, 5]. During the last decades, both the physics and the biology sides of the latter question have been completely transformed, especially by progress in imaging.

On the physics side, new so-called “complex” materials with an internal structure, such as foams, emulsions or gels, have been thoroughly studied, especially in the last twenty years, with a strong emphasis on the difficult problem of the feedback between the microscopic structure and the mechanical response [6, 7]. The development of new tools to image the changes in the microstructure arrangement under well-controlled global stresses or deformations has provided a wealth of data. Modelling has played a crucial part *via* the determination of so-called “constitutive equations”. A constitutive equation characterises the local properties of a material within the framework of continuum mechanics. It relates dynamical quantities, such as the stress carried by the material, with kinematical quantities, *e.g.* the deformation (also called “strain”) or the deformation rate.

On the biology side, questions now arise regarding the interplay of cell scale behaviour and tissue scale mechanical properties, among which the following two examples.

A first question is: how does a collective behaviour, which is not obviously apparent at the cell scale, emerge at the tissue scale? Analyses of images and movies suggested that epithelia or whole embryos behave like viscous liquids on long time scales [8]. The physical origin and the value of the (effective) viscosity should be traced back to the cell dynamics: it can in principle incorporate contributions from ingredients such as cell divisions and apoptoses [9] or cell contour fluctuations [10, 11], but also from orientational order, cell contractility, cell motility or cell rheological properties. All these local and sometimes changing ingredients become progressively accessible to experimental measurements. Biomechanical models can investigate the bottom-up relationship between local cell scale structure and tissue scale mechanical behaviour, unraveling the signature of the cellular structure in the continuum mechanics descriptions [10, 11].

A second question is: how can the mechanical state of the tissue have an influence on the cell division rate [12, 13], or on the orientation of the cells undergoing division [14]? In addition, the mechanical state of the tissue can generate cell polarity and hence an anisotropy of the local cell packing, which may affect the mutual influence between the local mechanics (forces and deformations) and the cell behaviour. Biomechanical models contribute to disentangle these complex feedback loops and address such top-down relationships.

To address these questions, a natural strategy is first to reconstruct the mechanics from the structural description, then to investigate the feedback between well-identified mechanical variables and the expression of specific genes. In particular, this interplay between genes and mechanics is expected to be the key to the spontaneous construction

of the adult form in a developing tissue without an organising center. Such problem in its full complexity will probably require a “systems biology” approach based on large scale mapping of expression for at least tens of genes, coupled to a correct mechanical modelling on an extended range of scales in time and space, which in turn supposes experimental setups able to produce the relevant genetic and mechanical data.

1.2 State of the art

Recent developments in *in vivo* microscopy yield access to the same richness of structural information for living tissues as has already been the case for complex fluids. The biology of cells and tissues is now investigated in detail in terms of protein distribution and gene expression, especially during development [15]. It is possible to image the full geometry of a developing embryonic tissue at cellular resolution [16–20], while visualising the expression of various genes of interest [21–23]. Mechanical fields such as the deformation, deformation rate or plastic deformation rate are increasingly accessible to direct measurement. Several fields can be measured quantitatively at least up to an unknown prefactor. This is the case for: distributions of proteins (involved in cytoskeleton, adhesion or force production), *via* quantitative fluorescence [24]; elastic forces and stresses, either by laser ablation of cell junctions [25] and tissue pieces [26], or through image-based force inference methods [27–30]; even viscous stress fields, indirectly estimated [23]. Other methods include absolute measurements of forces based on micro-manipulation [31], *in situ* incorporation of deformable force sensors [32] or fluorescence resonance energy transfer (FRET) [33].

In vitro assemblies of cohesive cells are useful experimental materials. Within a reconstructed cell assembly, each individual cell retains its normal physiological behaviour: it can grow, divide, die, migrate. In the absence of any regulatory physiological context, cells display small or negligible variation of gene expression. Reconstructed assemblies thus allow to separate the mechanical behaviour of a tissue from its feedback to and from genetics. Furthermore, in the absence of any coordinated variation of the genetic identity of constituent cells, spatial homogeneity may be achieved. Simple, well-controlled boundary conditions can be implemented by a careful choice of the geometry, either in two or three dimensions.

In two dimensions, confluent monolayers are usually grown on a substrate used both as a source of external friction and as a mechanical sensor to measure local forces [34–36]. 2D monolayers facilitate experiments, simulations, theory and their mutual comparisons [37–41]. 2D images are easier to obtain and can be analysed in detail; data are more easily manipulated, both formally and computationally.

In three dimensions, multi-cellular spheroids in a well-controlled, *in vitro* setting [10, 12, 42, 43] are a good material to mimic the mechanical properties of tumors, and of homogeneous parts of whole organs, either adult or during development. They are also useful for rheological

studies [44,45], especially since they are free from contact with a solid substrate. Although the full reconstruction of the geometry of multi-cellular spheroids at cellular resolution remains challenging, it has progressed in recent years [46].

1.3 Outline of the paper

A tissue can be seen as a cellular material, *active* in the sense that it is out of equilibrium due to its reservoir of chemical energy, which is converted into mechanical work at or below the scale of the material's constituents, the cells. A consequence of this activity is that force dipoles, as well as motion, are generated autonomously.

Our global strategy is as follows. We construct *rheological diagrams* based on insights concerning the mechanics of the biological tissue of interest. One of the main insights is a distinction between intra-cell mechanisms: elasticity, internal relaxation, growth, contractility, and inter-cell mechanisms: cell-cell rearrangement, division and apoptosis. The transcription of the rheological diagrams within the *dissipation function formalism* provides local rheological equations. We show how this local rheology should be inserted into the balance equations of continuum mechanics to generate a complete spatial model expressed as a *set of partial differential equations*. This procedure is conducted not only in the usually treated case of small elastic deformations, but also in the relevant, less discussed, case of large elastic deformations.

Our hope is to provide a functional and versatile toolbox for tissue modelling. We would like to guide the choice of approaches and of models according to the tissue under consideration, the experimental set-up, or the scientific question raised. We propose a framework for a tensorial treatment of spatially heterogeneous tissues. It is suitable to incorporate the data arising from the analysis of experimental data, which are increasingly often live microscopy movies. Although the simplest applications concern *in vitro* experiments, often performed with epithelial cells, the same approach applies to a wide spectrum of living tissues including animal tissues during development, wound healing, or tumorigenesis.

This article is organised as follows. Section 2 makes explicit our assumptions and arguments, then details the use of the dissipation function formalism. Section 3 reviews mechanical ingredients suitable for the theoretical description of a wide range of living tissues, both *in vitro* and *in vivo*, illustrated with worked out examples chosen for their simplicity. Section 4 groups these ingredients to form models of more realistic applications. Section 5 summarizes and opens perspectives.

Appendix A examines the link between the scale of discrete cells and the scale of the continuous tissue. Appendix B provides more details on how to write and use equations within the dissipation function formalism. Appendix C provides further examples of coupling with non-mechanical fields. Appendix D examines the requirements to treat tissue mechanics at large deformation.

2 Choices and methods

In this section, we explain our choices and our assumptions. Section 2.1 compares discrete and continuum approaches. Section 2.2 compares rheological diagrams, hydrodynamics, and the dissipation function formalisms. Section 2.3 discusses specific requirements to model cellular materials. Section 2.4 suggests how to incorporate space dependence in constitutive equations to write partial differential equations.

2.1 A continuum rather than a discrete description

Models that describe tissue mechanical properties may be broadly split into two main categories: bottom-up “cell-based” simulations and continuum mechanics models.

Direct cellular simulations are built upon the (supposedly known) geometry and rheology of each individual cell and membrane. They generate a global tissue behaviour through the computation of the large-scale dynamics of assemblies of idealised cells [47–57]. Simulations enable to directly test the collective effect of each cell scale ingredient, and of their mutual feedbacks. Also, they work well over a large range of cell numbers, up to tens of thousands, and down even to a small number of cells, where the length scale of a single cell and that of the cell assembly are comparable.

A continuum approach requires the existence of an intermediate length scale, larger than a typical cell size, yet smaller than the tissue spatial extension, and beyond which the relevant fields vary smoothly. The continuum rheology is captured through a constitutive equation relating the (tensorial) stresses and deformations [58–66]. This rheological model is incorporated into the usual framework of continuum mechanics using fundamental principles such as material and momentum conservation. Note that continuum models have also been applied to vegetal tissues, as in plant growth [58,67].

Both categories are complementary and have respective advantages. For the purpose of the present paper, we favor the continuum approach, which incorporates more easily precise details of cellular rheology. When it succeeds, a continuum approach yields a synthetic grasp of the relevant mechanical variables on an intermediate scale (*i.e.* averaged over many individual cells), and helps dealing with large tissues. It often involves a smaller number of independent parameters than a discrete approach, and this helps comparing with experimental observations.

In order to test and calibrate a continuum model, it is generally necessary to extract continuum information from other sources such as discrete simulations or experiments on tissues with cell scale resolution. Analysis tools have been developed in recent years to process segmented experimental movies in order to extract tensorial quantities from cell contours, which might include the elastic deformation and the plastic deformation rate [68]; for completeness, these tools are recalled in appendix A.1.

The continuum models describing amorphous cellular materials can be tensorial and can incorporate viscoelasto-

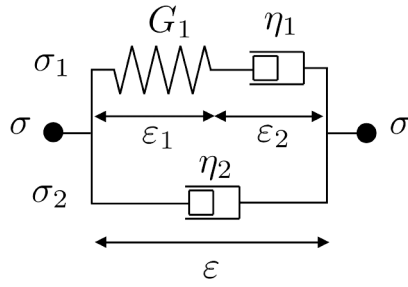


Fig. 1. An example of a rheological diagram: the Oldroyd viscoelastic fluid model [73]. A Maxwell element (spring of stiffness G_1 in series with a dashpot of viscosity η_1) is in parallel with a dashpot of viscosity η_2 .

plastic behaviour [58,64,69–71]. In addition to the viscous and elastic behaviour expected for a complex fluid that can store elastic deformation in its microstructure, one incorporates the ingredient of plasticity. It captures irreversible structural changes, more specifically here i) local rearrangements of the individual cells (see fig. 2) ii) cell division or iii) plasticity within the cell. A viscoelastoplastic model assembling these ingredients could capture the different “short-time” phenomena described in sect. 3 and at the same time display a viscous liquid-like behaviour on longer time scales.

In the following, we choose to concentrate on continuum models, drawing inspiration both from models of (non-living) amorphous cellular materials such as liquid foams [72], and from models of living matter that incorporate ingredients such as cell division [9] and orientational order [65,66].

2.2 Choice of the dissipation function formalism

In this section, we discuss three complementary general formalisms used to construct constitutive equations, indifferently in two or three dimensions: rheological diagrams (sect. 2.2.1), hydrodynamics in its general sense (sect. 2.2.2) and dissipation function (sect. 2.2.3). For simplicity we consider here stress and other mechanical tensors only with symmetrical components, while in general these three formalisms can include antisymmetric contributions when required.

2.2.1 Rheological diagram formalism

Figure 1 represents a classical example of rheological diagram: the Oldroyd viscoelastic fluid model [73]. It consists in a dashpot with viscosity η_2 and deformation ε carrying the stress σ_2 in parallel with a Maxwell element carrying the stress σ_1 . This Maxwell element is itself made of a spring (stiffness G_1 , deformation ε_1) in series with a dashpot (viscosity η_1 , deformation ε_2). The elementary

rheological equations read

$$\begin{aligned}\varepsilon &= \varepsilon_1 + \varepsilon_2, \\ \sigma &= \sigma_1 + \sigma_2, \\ \sigma_2 &= \eta_2 \dot{\varepsilon}, \\ \sigma_1 &= G_1 \varepsilon_1, \\ \sigma_1 &= \eta_1 \dot{\varepsilon}_2.\end{aligned}\quad (1)$$

Eliminating ε_1 , $\dot{\varepsilon}_1$, ε_2 and $\dot{\varepsilon}_2$ between eqs. (1) yields

$$\dot{\sigma} + \frac{G_1}{\eta_1} \sigma = \frac{\eta_1 + \eta_2}{\eta_1} G_1 \dot{\varepsilon} + \eta_2 \ddot{\varepsilon}.\quad (2)$$

Equation (2) is a constitutive equation for the ensemble. Such a straightforward method is useful when physical knowledge or intuition of the material and its mechanical properties is sufficient to determine the topology (nodes and links) of the diagram.

Note that the relationship between a rheological diagram and a constitutive equation is *not* one-to-one. For instance, a Maxwell element (linear viscoelastic liquid) in *parallel* with a dashpot is a diagram distinct from a Voigt element (linear viscoelastic solid) in *series* with a dashpot, but both are associated to the same constitutive equation. Section 3.3 presents another example.

2.2.2 Hydrodynamic formalism

When non-mechanical variables are present, the rheological diagram formalism (sect. 2.2.1) is not sufficient to establish the constitutive equation. Another formalism is necessary to include couplings between mechanical and non-mechanical variables.

A possible formalism is linear out-of-equilibrium thermodynamics, also called “hydrodynamics” [74] although its range of application is much larger than the mechanics of simple fluids. This approach has been highly successful, leading for instance to the derivation of the hydrodynamics of nematic liquid crystals (with the nematic director field as an additional, non-conserved hydrodynamic variable) [75,76]; the collective movements of self-propelled particles [77,78] (which have been suggested to be analogous with tissues dynamics [56]); or, more recently, of soft active matter (where a chemical field typically couples to an orientational order parameter to be modeled separately, *e.g.* cytoskeletal mechanics) [79,80].

Broadly speaking, hydrodynamics may be defined as the description of condensed states of matter on slow time scales and at large length scales. Macroscopic behaviour is characterized by the dynamics of a small number of slow fields (so-called “hydrodynamic fields”), related to conservation laws and broken continuous symmetries [74]. On time scales long compared to the fast relaxation times of microscopic variables, the assumption of local thermodynamic equilibrium leads to the definition of a thermodynamic potential as a function of all relevant (long-lived) thermodynamic variables and their conjugate quantities. Standard manipulations lead to the expression of the entropy creation rate as a bilinear functional of generalized

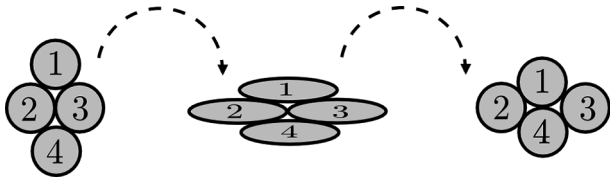


Fig. 2. Cell rearrangement, also known as: intercalation, neighbour exchange, or T1 process [21,72]. Cells 2 and 3 are initially in contact (left). Cells deform (center) and can reach a configuration with a new topology where cells 1 and 4 are now in contact, then relax (right).

fluxes and forces. In the vicinity of thermodynamical equilibrium, generalized fluxes are expressed as linear combinations of generalized forces. Due to microreversibility, the Onsager symmetry theorem implies that cross-coefficients must be set equal (respectively, opposite) when fluxes and forces have equal (respectively, opposite) sign under time reversal [81,82].

The hydrodynamic formalism is physically intuitive. It is flexible and can accommodate a broad spectrum of physical quantities, as long as deviations from equilibrium can be linearised. This approach is quite general since it relies on thermodynamic principles and on the invariance properties of the problem under consideration. Constitutive equations may thus be written within the domain of linear response as linear relationships between generalized fluxes and forces.

2.2.3 Dissipation function formalism

However, not all materials are described by a linear force-flux relationship. In tissues, plastic events such as cell rearrangements (fig. 2) have thresholds which break down the linearity, and hydrodynamics (sect. 2.2.2) becomes inadequate. Deriving constitutive equations requires a more general formalism.

In the dissipation function formalism, the state of the material is described by the total deformation ε and by $m \geq 0$ additional, independent, internal variables ε_k , with $1 \leq k \leq m$. These variables may be scalar, vectorial or tensorial. So-called “generalized standard materials” are defined by the existence of the energy function \mathcal{E} and the dissipation function \mathcal{D} , which are continuous (not necessarily differentiable) and convex functions of their respective arguments [83–85]:

$$\mathcal{E} = \mathcal{E}(\varepsilon, \varepsilon_1, \dots, \varepsilon_m), \quad (3)$$

$$\mathcal{D} = \mathcal{D}(\dot{\varepsilon}, \dot{\varepsilon}_1, \dots, \dot{\varepsilon}_m). \quad (4)$$

Here $\dot{\varepsilon}$ denotes the total deformation rate, and $\dot{\varepsilon}_k$ is the (Lagrangian) time derivative of ε_k . Although it is rarely explicitly stated, these energy and dissipation functions should increase when the norms of their arguments tend to infinity, so that they admit one (and only one) minimum, reached for a finite value of their arguments. Constitutive and evolution equations are obtained through the

following rules, where σ denotes the stress:

$$\sigma = \frac{\partial \mathcal{D}}{\partial \dot{\varepsilon}} + \frac{\partial \mathcal{E}}{\partial \varepsilon}, \quad (5)$$

$$0 = \frac{\partial \mathcal{D}}{\partial \dot{\varepsilon}_k} + \frac{\partial \mathcal{E}}{\partial \varepsilon_k}, \quad 1 \leq k \leq m. \quad (6)$$

Appendix B provides more details on how to use the dissipation function formalism. In particular, appendix B.1 explains how to manipulate the corresponding equations. Appendix B.2 explicitly treats the tensorial case, and shows that the tensorial variables in eqs. (3), (4) should be decomposed into their trace and deviatoric parts:

$$\mathcal{E} = \mathcal{E}(\text{tr } \varepsilon, \text{tr } \varepsilon_1, \dots, \text{dev } \varepsilon, \text{dev } \varepsilon_1, \dots), \quad (7)$$

$$\mathcal{D} = \mathcal{D}(\text{tr } \dot{\varepsilon}, \text{tr } \dot{\varepsilon}_1, \dots, \text{dev } \dot{\varepsilon}, \text{dev } \dot{\varepsilon}_1, \dots), \quad (8)$$

considered as independent variables. Appendix B.3 explicits the incompressible case.

The formalism of eqs. (3)–(6) is a convenient tool for building complex models and obtaining in a systematic way the full set of partial differential equations from simple and comprehensive graphical schemes. The coupling coefficients arise as cross partial derivatives, with the advantage that they derive from a smaller number of free parameters than in the hydrodynamics formalism.

For purely mechanical diagrams made of springs, dashpots and sliders, the dissipation function formalism yields the same equations as when directly writing the dynamical equations from the rheological model, as shown in appendix B.4. The same formalism also applies to systems with non-mechanical variables, see sect. 3.4 and appendix C.

A direct link between the hydrodynamic and dissipation function formalisms can be established when the dissipation function \mathcal{D} is a quadratic function of its arguments. For a given variable ε_k , quadratic terms ε_k^2 in the energy function or $\dot{\varepsilon}_k^2$ in the dissipation function are harmonic, *i.e.* they yield a linear term ε_k or $\dot{\varepsilon}_k$ in the derived dynamical equations, exactly like in the hydrodynamics formalism (sect. 2.2.2). In this case, \mathcal{D} is proportional to the rate of entropy production [82] (this is also true for viscoplastic flows [86]).

The dissipation function formalism is also suitable for nonlinear terms. Terms of the form $|\varepsilon_k|^n$ or $|\dot{\varepsilon}_k|^n$, with $n \geq 1$ (n integer or real) yield nonlinear terms $|\varepsilon_k|^{n-2}\varepsilon_k$ or $|\dot{\varepsilon}_k|^{n-2}\dot{\varepsilon}_k$ in the dynamical equations.

Interestingly, the dissipation function can even include the particular case $n = 1$ which corresponds to terms like $|\varepsilon_k|$ or $|\dot{\varepsilon}_k|$. This yields terms of the form $\varepsilon_k/|\varepsilon_k|$ or $\dot{\varepsilon}_k/|\dot{\varepsilon}_k|$ in the derived equations: these are nonlinear terms which dominate over the linear ones. This lowest-order case is useful to include plasticity (see sect. 3.1 for an example), whose treatment thus becomes straightforward [84–86]: the dissipation function formalism has been successfully applied to viscoelastoplastic flows [87,88]. As discussed in sect. 3.1, regularizing such terms would suppress yield stress effects.

Since the cross coupling coefficients arise as cross partial derivatives, they are by construction always equal by

pairs. The Onsager symmetry theorem [81] is thus immediately obeyed when fluxes and forces behave similarly under time reversal, but not if they behave differently. Note that this is compatible with the constitutive equations of living tissues: since microreversibility may not apply at the (cell) microscale, the Onsager symmetry theorem does not need to apply.

Active ingredients which impose a force, a deformation rate, or a combination thereof, can be included in the dissipation function formalism, as shown for instance in sect. 3.3. The functions \mathcal{E} and \mathcal{D} remain convex and still reach a minimum for a finite value of their arguments. As expected, the entropy creation rate is no longer always positive.

From a mathematical point of view, the large set of nonlinear differential equations is known to be well posed in the Eulerian and small deformation setting [89]. Since the free energy function \mathcal{E} and the dissipation function \mathcal{D} are both convex, in the case of small deformations the existence and uniqueness of solution is guaranteed, while the second law of thermodynamics is automatically satisfied [83,85]. This is a major advantage of the dissipation function framework.

In addition, the formalism is also effective from a computational point of view. For problems which involve multi-dimensional and complex geometries together with large deformations of the tissue, there is no hope to obtain an explicit expression of the solution: its computation should be obtained by an approximation procedure. The resolution of the large set of nonlinear differential equations and its convergence at high accuracy require both a dedicated algorithm and a large computing time with the present computers. The convexity of \mathcal{E} and \mathcal{D} functions enables to use robust optimization algorithms to solve efficiently the set of dynamical equations thanks to variational formulations [90,91]. This second major advantage of the dissipation function framework has been widely used in small deformation, for applications in solid mechanics and plasticity, and has allowed the development of robust rocks and soils finite element modeling softwares (see *e.g.* [86,89] and references therein).

In summary, since the dissipation function formalism allows to treat plasticity and is convenient for numerical resolution, we recommend to adopt it for living tissues.

2.3 Specificity of cellular material modelling

While continuum mechanics is standard, cellular material modelling requires care on specific points. They include: the separation of the deformation between its contribution arising from inside each cell and from the mutual cell arrangement (sect. 2.3.1); the choice of Eulerian rather than Lagrangian description for a viscous, elastic, plastic material (sect. 2.3.2); and the treatment of large elastic deformations (sect. 2.3.3).

2.3.1 Intra-cell and inter-cell deformation

Different deformation rates can be measured simultaneously and independently (see appendices A.1 and D.1).

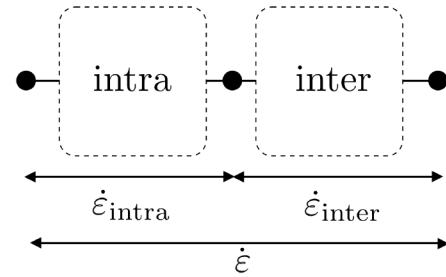


Fig. 3. Decomposition of the tissue deformation rate $\dot{\epsilon}$ into the deformation rate $\dot{\epsilon}_{\text{intra}}$ of the constituent cells and the deformation rate $\dot{\epsilon}_{\text{inter}}$ that reflects inter-cell relative velocities (eq. (9)).

The total deformation rate $\dot{\epsilon}$ can be measured by tracking the movements of markers, moving with the tissue as if they were pins attached to the tissue matter. This total deformation rate originates from the following two contributions at the cellular level.

The intra-cellular deformation rate $\dot{\epsilon}_{\text{intra}}$ is the average of the deformation rate as perceived by individual cells, where each cell is only aware of the relative positions of its neighbours. The intra-cellular deformation ϵ_{intra} can be measured by observing the anisotropy of a group of tracers attached to a reference cell and its neighbours, followed by an average over reference cells. By contrast with $\dot{\epsilon}$, the tracers are not attached permanently to the tissue itself: when neighbours rearrange and lose contact with the reference cell, the corresponding tracers are switched immediately to the new neighbours. The intra-cell deformation rate $\dot{\epsilon}_{\text{intra}}$ is then obtained as the rate of change of this intra-cell deformation measure ϵ_{intra} .

The inter-cellular deformation rate $\dot{\epsilon}_{\text{inter}}$ reflects the cell rearrangements and relative movements. It can be measured by tracking the rearrangements themselves.

In tissues made of cells which tile the space, the stress at the tissue scale is the stress carried by the cells themselves (like in foams, but as opposed *e.g.* to the case of plants, where the rigid walls are as important as pressure for stress transmission). We thus advocate a decomposition in series, where intra- and inter-cellular stresses are equal, while intra- and inter-cellular deformation rates add up (fig. 3):

$$\dot{\epsilon} = \dot{\epsilon}_{\text{intra}} + \dot{\epsilon}_{\text{inter}}. \quad (9)$$

Choosing this decomposition into intra-cell and inter-cell contributions in series has consequences on the arguments of the dissipation function. When defining the ϵ_k variables, see eqs. (3), (4), it is relevant to choose one of them as equal to ϵ_{intra} . Appendix D.1.2 discusses the case of large deformations.

2.3.2 An Eulerian rather than a Lagrangian approach

We now compare the Lagrangian and Eulerian points of view, and explain why we choose the latter.

For materials that retain information about their initial state, it is natural (and common) to use a deformation

variable, often denoted ε , that compares the current local material state to the initial state of the same material region. This is called the Lagrangian description and is usually preferred for elastic solids [92]. The deformation rate $\dot{\varepsilon}$ of the Lagrangian description is the time derivative of the deformation ε , where the dot denotes the material derivative used for small deformations, $\partial_t + \mathbf{v} \cdot \nabla$:

$$\dot{\varepsilon} = \frac{\partial \varepsilon}{\partial t} + \mathbf{v} \cdot \nabla \varepsilon. \quad (10)$$

On the other hand, when plastic or viscous flows erase most or all memory of past configurations, it is common practice to use only the current velocity field $\mathbf{v}(\mathbf{x}, t)$ as the main variable, with no reference to any initial state. This is called the Eulerian description, used for instance when writing the Navier-Stokes equations.

Both descriptions are tightly connected: the deformation rate $\dot{\varepsilon}$ of the Lagrangian description is equal to the (symmetric part of the) gradient of the velocity field $\mathbf{v}(\mathbf{x}, t)$ of the Eulerian description:

$$\dot{\varepsilon} = \frac{\nabla \mathbf{v} + \nabla \mathbf{v}^T}{2}. \quad (11)$$

See eqs. (D.6), (D.8) for the complete expression at large deformations.

The separation of intra- and inter-cellular dynamics, discussed in sect. 2.3.1, can be viewed as mixing the Lagrangian and Eulerian points of view. Since cells retain their integrity, the quantity $\varepsilon_{\text{intra}}$ is similar to a deformation variable in a Lagrangian approach. By contrast, the relative motions of cells (described by $\dot{\varepsilon}_{\text{inter}}$) is similar to the relative motions of material points in usual fluids, described from an Eulerian point of view.

A globally Eulerian description has been implemented for liquid foams in a direct manner, based on the argument that the rearrangement deformation rate $\dot{\varepsilon}_{\text{inter}}$ progressively erases from the material the memory of the initial configuration and thus progressively wipes, like in common fluids, the relevance of the material deformation ε for predicting the future evolution of the material [69].

Here, the same argument should apply. In the examples provided in sect. 3 the variables $\varepsilon_{\text{inter}}$ and ε naturally disappear from the final constitutive equation, and only their corresponding deformation rates $\dot{\varepsilon}_{\text{inter}}$ and $\dot{\varepsilon}$ contribute. This reflects the absence of any structure holding cells together beyond the first neighbours. It confirms the relevance of an Eulerian description for a material such as a tissue.

2.3.3 Large elastic deformations

For pedagogical reasons, in the present article, all equations are written within the limit of small elastic deformations. Yet, in living tissues, large elastic deformations are encountered.

Appendix D explains in details how to model large deformations in the specific context of tissue mechanics, and

reformulate accordingly the dissipation function formalism. In particular, it discusses the volume evolution, the elasticity and its transport, and the intra-cell deformation.

An example of changes due to large deformations is the distinction between two quantities which are equal in the limit of small deformations (eq. (11)): the deformation rate and the symmetrised velocity gradient (eqs. (D.6), (D.8)). The transport of large elastic deformations involves objective derivatives. Several such derivatives exist, for instance lower- and upper-convected derivatives, as well as Gordon-Schowalter derivatives which interpolate between them. In rheological studies of complex fluids, the selection of the derivative is often motivated by formal reasons, or is empirical. In appendix D.1.1, for physical reasons, we describe the deformation using tensors attached to the cellular structure; we show that this choice selects univocally the upper-convected derivative.

2.4 Set of partial differential equations

A tissue may be spatially heterogeneous: its material properties, its history, its interaction with its environment are under genetic control and may depend on the position \mathbf{x} . For instance the tissue may comprise different cell types, or it may be placed on a spatially modulated substrate.

The parameters and variables which describe the tissue are fields that may vary spatially. Here, we consider only tissues amenable to a continuum mechanics description, namely tissues whose relevant fields are smooth and slowly variable over the scale of a group of cell (the ‘‘representative volume element’’ of the continuum mechanics description). In what follows, we assume that the fields are continuous and differentiable.

The evolution of the tissue is then expressed as a set of partial differential equations (PDE), consisting in conservation laws and constitutive equations. To make this article self-contained, we show in the present Section how constitutive relations, such as derived using the dissipation function formalism, can be embedded in the rigorous framework of continuum mechanics in order to obtain a closed set of evolution equations.

In continuum mechanics, one usually starts from the conservation equations of mass, momentum and angular momentum. The mass conservation equation reads

$$\frac{\partial \rho}{\partial t} + \nabla \cdot (\rho \mathbf{v}) = s, \quad (12)$$

where ρ is the mass density (or mass per unit area in 2D); and s represents material sources or sinks which, in the context of a tissue, can be linked with cell growth and apoptosis, respectively, see sect. 3.2.2.

In general, the conservation of momentum reads:

$$\rho \mathbf{a}(\mathbf{x}, t) = \nabla \cdot \boldsymbol{\sigma}(\mathbf{x}, t) + \mathbf{f}(\mathbf{x}, t) \quad (13)$$

which relates the acceleration $\mathbf{a} = \frac{\partial \mathbf{v}}{\partial t} + (\mathbf{v} \cdot \nabla) \mathbf{v}$ to the internal stress tensor $\boldsymbol{\sigma}$ and the external forces \mathbf{f} . For instance, the external force \mathbf{f} may contain a friction component $\mathbf{f} = -\zeta \mathbf{v}$ [26, 38, 41]. Note that, in a tissue, the inertial term $\rho \mathbf{a}$ is generally negligible when compared to the

stress term $\nabla \cdot \sigma$. The validity of this approximation has to be checked in specific examples by estimating the value of the relevant dimensionless number, *e.g.* the Reynolds number for a purely viscous material, or the elastic number for a purely elastic solid. In this case, the conservation of momentum (eq. (13)) reads

$$\nabla \cdot \sigma(\mathbf{x}, t) + \mathbf{f}(\mathbf{x}, t) = \mathbf{0}. \quad (14)$$

Finally, the conservation of angular momentum implies that the stress tensor is symmetric [74]: $\sigma_{ij} = \sigma_{ji}$.

We obtain a set of $m + 4$ evolution equations (eqs. (5), (6), (11), (12), (14)). There are $m + 4$ unknown fields: σ , $(\varepsilon_k)_{1 \leq k \leq m}$, ε , ρ and \mathbf{v} . For any value d of the space dimension, the number of coordinates of the unknown fields always equals the number of equations. This set of partial differential equations is closed by suitable initial conditions on the same variables and d boundary conditions in terms of velocity, deformation and/or stress components. Its solution can be estimated by numerical resolution: see *e.g.* [70,90,91,93,94] for such numerical methods in the context of liquid foam flows.

3 Ingredients included in tissue modelling

A (non-exhaustive) list of ingredients for tissue modelling includes viscosity, elasticity, plasticity, growth, contractility, chemical concentration fields, cell polarity, and their feedbacks. Note that other tissue-specific ingredients such as (possibly active) boundary conditions [41] do not contribute to constitutive equations themselves: they are used to solve the set of partial differential equations (established in sect. 2.4).

In sects. 3.1 to 3.4, we present four worked out examples showing how such ingredients are taken into account within the dissipation function formalism. Each choice in this section is motivated by the simplicity (rather than by the formalism, as in sect. 2, or by the realism, as in sect. 4). Section 3.5 combines individual ingredients into a composite rheological model by classifying them in terms of shape or volume contributions at the intra-cell or inter-cell level, and derives the corresponding set of equations.

3.1 Plasticity

3.1.1 Rearrangements and plastic deformation rate

Recent experiments performed on cell aggregates and cell monolayers have shown that these tissues can have a yield stress [39,45] and display a plastic behavior [10,95]. The origin of this plasticity includes cell rearrangements (fig. 2) [96,97] which also play an important role during development, as in *e.g.* convergence-extension [15].

At the cell scale, and independently of its biological origin and regulation, a cell rearrangement is mathematically speaking a discontinuous topological process in a group of neighbouring cells. The associated mechanical description

is decomposed into several steps. Before the rearrangement, the cells deform viscoelastically. During the rearrangement, two cells in contact get separated. Both other cells establish a new contact. They all eventually relax towards a new configuration with the consequence that two cells have got closer while the others have moved apart.

Upon coarse-graining spatially at a scale of several cells, and temporally over a time scale much larger than the relaxation time, the discontinuities at the cell scale are wiped out. The net result is an irreversible change in the stress-free configuration of the tissue, with convergence along one axis and extension along the perpendicular one. It is thus best described as a tensor with positive and negative eigenvalues [68,69], which tends towards the plastic deformation rate $\dot{\varepsilon}_p$ in the continuum limit. This tensor is the difference between the total deformation rate $\dot{\varepsilon}$ and the elastic deformation rate $\dot{\varepsilon}_e$, so that the cumulated effect of elastic and plastic contributions add up:

$$\dot{\varepsilon} = \dot{\varepsilon}_e + \dot{\varepsilon}_p. \quad (15)$$

3.1.2 Plasticity and dissipation function

In the dissipation function formalism, elastoplastic and viscoelastoplastic materials are classically described by adding in the dissipation energy a yield stress term, for instance proportional to the norm of the deformation rate (sect. 2.2.3). Such non-analytic term is fully compatible with the formalism. The convexity of the energy function is preserved, so that equations are readily written and can be solved using known numerical approaches. For details, see ref. [98].

When writing equations, physicists often favor smooth (analytic) expressions rather than discontinuous (singular) ones. Formally, it would of course be possible to regularize the plasticity equations and obtain a differentiable dissipation function by replacing each non-analytical term with analytic, strong non-linearities. However, this would lead to a completely different category of models, from which yield stress effects are absent and the solid behaviour vanishes in the long time limit.

3.1.3 A viscoelastoplastic example

We treat explicitly an example obtained by adding an elastic element of modulus G in series with a diagram representing a Bingham fluid, namely the combination in parallel of a dashpot of viscosity η and a slider of yield stress σ_Y (fig. 4). A more realistic (and therefore more complex) rheological model of a tissue that includes plasticity is treated in sect. 4.1.

According to fig. 4, we have

$$\varepsilon = \varepsilon_1 + \varepsilon_2. \quad (16)$$

Choosing ε and ε_2 as independent variables, the energy function reads

$$\mathcal{E}(\varepsilon, \varepsilon_2) = \frac{1}{2} G \varepsilon_1^2 = \frac{1}{2} G (\varepsilon - \varepsilon_2)^2 \quad (17)$$

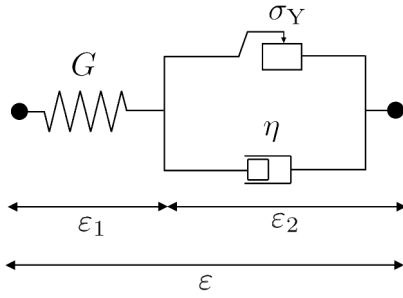


Fig. 4. Rheological diagram for a plastic material. An elastic element of modulus G is in series with a viscoplastic (Bingham) fluid, namely a dashpot of viscosity η in parallel with a slider of yield stress σ_Y .

and the dissipation function

$$\mathcal{D}(\dot{\varepsilon}, \dot{\varepsilon}_2) = \frac{1}{2} \eta \dot{\varepsilon}_2^2 + \sigma_Y |\dot{\varepsilon}_2|. \quad (18)$$

From eqs. (5), (6) we obtain

$$\sigma = \frac{\partial \mathcal{D}}{\partial \dot{\varepsilon}} + \frac{\partial \mathcal{E}}{\partial \varepsilon} = G(\varepsilon - \varepsilon_2), \quad (19)$$

$$0 = \frac{\partial \mathcal{D}}{\partial \dot{\varepsilon}_2} + \frac{\partial \mathcal{E}}{\partial \varepsilon_2} = \eta \dot{\varepsilon}_2 + \sigma_Y \frac{\dot{\varepsilon}_2}{|\dot{\varepsilon}_2|} - G(\varepsilon - \varepsilon_2), \quad (20)$$

which together yields the constitutive equation

$$\sigma = \sigma_Y \frac{\dot{\varepsilon}_2}{|\dot{\varepsilon}_2|} + \eta \dot{\varepsilon}_2. \quad (21)$$

When $\dot{\varepsilon}_2 = 0$, σ takes a value in the interval $[-\sigma_Y; +\sigma_Y]$: for a rigorous mathematical analysis, see ref. [88], and in particular its eqs. (9), (10).

3.2 Growth

3.2.1 Conservation equations

The growth of a tissue has two aspects: mass growth and cell concentration growth. The mass growth affects the mass conservation (eq. (12)) through its source term $s = \alpha_g \rho$, where α_g is the rate of variation of mass density, which has the dimension of an inverse time

$$\partial_t \rho + \text{div}(\rho \mathbf{v}) = \alpha_g \rho. \quad (22)$$

Similarly, the cell concentration c (number of cells per unit volume) evolves according to

$$\partial_t c + \text{div}(c \mathbf{v}) = \alpha_c c, \quad (23)$$

where α_c is the rate of variation of the cell concentration.

If we consider a tissue without gaps between cells, it is reasonable to write that the mass density ρ is a constant, which simplifies the description. Equation (22) reduces to

$$\text{div}(\mathbf{v}) = \alpha_g. \quad (24)$$

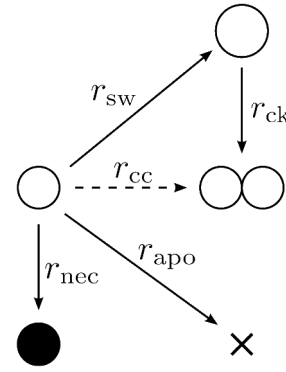


Fig. 5. Cell growth modes in a tissue. Cells may swell (rate r_{sw}); undergo cytokinesis (rate r_{ck}); or both successively, resulting in a cell cycle (rate r_{cc}). They may die by apoptosis (rate r_{apo}) or necrosis (rate r_{nec}).

Equation (A.7) indicates how to locally measure α_g . For a monolayer of varying thickness h but homogeneous and constant density ρ , eq. (22) can be rewritten using the two-dimensional divergence applied in the plane of the monolayer, div_{2d}

$$\partial_t h + \text{div}_{2d}(h \mathbf{v}) = \alpha_g h. \quad (25)$$

3.2.2 Cell growth modes

Several cell processes alter the tissue volume, the cell concentration, or both (fig. 5). They are compatible with the dissipation function formalism, see for instance sect. 4.2.1. All rates are noted r and have the dimension of the inverse of a time (for instance typically a few hours or a day for the division rate of epithelial cells in vitro [99]). For each process, the corresponding r is the proportion of cells that undergo the process per unit time. Each process becomes relevant as soon as the duration of an experiment is of the order of, or larger than, the inverse of its rate r .

Cells may grow, *i.e.* swell, with rate r_{sw} , which creates volume and decreases c . They may undergo cytokinesis, *i.e.* split into daughter cells, which increases c with rate r_{ck} (c doubles in a time $\ln 2/r_{ck}$) without altering the volume. In the case where the swelling and cytokinesis rates are equal, and their common value is the cell-cycle rate $r_{cc} = r_{sw} = r_{ck}$, the long-time average of cell size is constant. For simplicity, the description of cytokinesis proposed in this section is scalar. More generally, one may need to define a tensor $\dot{\varepsilon}_{ck}$, with $r_{ck} = \text{tr} \dot{\varepsilon}_{ck}$ (see sect. 3.5.1).

Cells may undergo necrosis (rate r_{nec}), which does not alter the tissue volume but decreases the concentration c of living cells. The description of apoptosis (rate r_{apo}), namely cell death under genetic control, requires some care. If the content of the apoptosed cell material is eliminated (for instance diffuses away, or is cleaned by macrophages) without being taken up by the neighbouring cells; and if we further assume that the tissue remains connective (*i.e.*, neighbouring cells move to span the emptied region); then apoptosis causes the tissue volume to decrease while c remains unaltered.

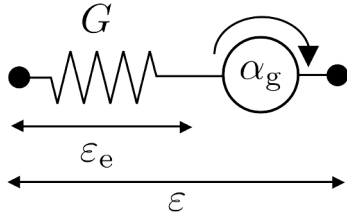


Fig. 6. Model for growth in the presence of elasticity. The active deformation rate, here the growth rate α_g , is constant, and the spring has a stiffness G .

The mass and cell concentration growth rates (defined in sect. 3.2.1) are

$$\alpha_g = r_{sw} - r_{apo}, \quad (26)$$

$$\alpha_c = r_{ck} - r_{sw} - r_{nec}. \quad (27)$$

A first special case is the situation where cells undergo cytokinesis without growing, hence leading to a decrease of the average cell size, as encountered for example during the first rounds of cytokineses in a developing embryo. In that case, only the cell concentration has a non-zero source, and eqs. (26), (27) reduce to

$$\alpha_g = 0, \quad (28)$$

$$\alpha_c = r_{ck}. \quad (29)$$

In the situation that combines cell swelling and cytokinesis at equal rates, in equal amounts, and in the presence of apoptosis, eqs. (26), (27) reduce to

$$\alpha_g = r_{cc} - r_{apo}, \quad (30)$$

$$\alpha_c = 0. \quad (31)$$

3.2.3 A one-dimensional example

We illustrate with a one-dimensional example the case where cell swelling and cytokinesis rates are equal, resulting in a constant long-time average cell size. Here, we assume that after a full cell cycle the rest length of each daughter cell, defined as the length where their elastic energy is lowest, is eventually identical to that of the mother cell. Appendix A.3 describes a tissue made of elastic cells which divide and/or die; it shows that the stress evolution equation reads

$$\dot{\sigma} \simeq G(\dot{\epsilon} - \alpha_g). \quad (32)$$

Equation (32) expresses that as expected, the stress (counted positive when tensile), increases when the tissue is subjected to elongation and decreases when the growth rate increases the tissue rest length [100,101].

Equation (32) can be derived from the rheological diagram shown in fig. 6, as follows. Consider a motor working at constant deformation rate, here the growth rate α_g , in series with a spring of stiffness G . It creates a difference between the total deformation rate $\dot{\epsilon}$ and the deformation rate $\dot{\epsilon}_e$ of the spring

$$\dot{\epsilon}_e = \dot{\epsilon} - \alpha_g. \quad (33)$$

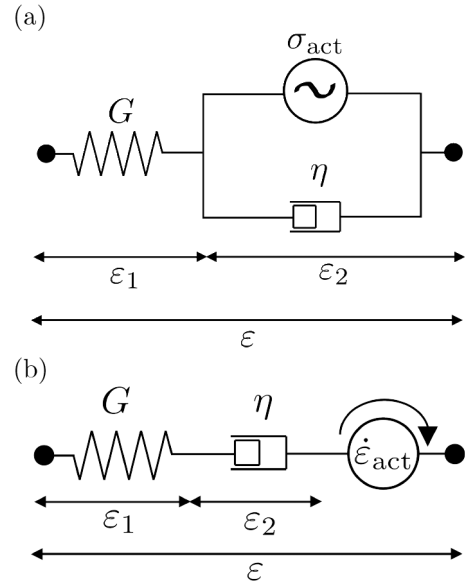


Fig. 7. Two equivalent models of contractility. (a) With a constant active stress σ_{act} . (b) With a constant active deformation rate $\dot{\epsilon}_{act}$.

Combined with the elasticity

$$\sigma = G\epsilon_e \quad (34)$$

this yields (32).

When used in the dissipation function formalism, eq. (33) which relates $\dot{\epsilon}_e$, $\dot{\epsilon}$ and α_g , is a topological relation and can be used in the same way as eq. (16).

3.3 Contractility

In tissues, cell scale contractility is often determined by the distribution of molecular motors such as myosin II. Upon coarse-graining, this distribution translates into tissue scale contractility. In one dimension, such contractility may be modelled by a constant stress, as done in classical models of muscle mechanics [102]. As an example, we study the rheological diagram of fig. 7a, where within a Maxwell model (spring and dashpot in series) a contractile element is placed in parallel with the dashpot.

Choosing ϵ and for instance ϵ_2 as independent variables (with $\epsilon = \epsilon_1 + \epsilon_2$), the energy and dissipation functions can be written in the form of eqs. (3), (4), with $m = 1$:

$$\mathcal{E}(\epsilon, \epsilon_2) = \frac{1}{2}G\epsilon_1^2 = \frac{1}{2}G(\epsilon - \epsilon_2)^2, \quad (35)$$

$$\mathcal{D}(\dot{\epsilon}, \dot{\epsilon}_2) = \frac{1}{2}\eta\dot{\epsilon}_2^2 + \sigma_{act}\dot{\epsilon}_2, \quad (36)$$

where σ_{act} denotes the active stress: it is positive in the case of a contracting tissue.

Equations (35), (36) injected into eqs. (5), (6) yield

$$\sigma = \frac{\partial \mathcal{D}}{\partial \dot{\varepsilon}} + \frac{\partial \mathcal{E}}{\partial \varepsilon} = G(\varepsilon - \varepsilon_2), \quad (37)$$

$$0 = \frac{\partial \mathcal{D}}{\partial \dot{\varepsilon}_2} + \frac{\partial \mathcal{E}}{\partial \varepsilon_2} = \eta \dot{\varepsilon}_2 - G(\varepsilon - \varepsilon_2) + \sigma_{\text{act}}. \quad (38)$$

Differentiating eq. (37) yields $\dot{\sigma} = G(\dot{\varepsilon} - \dot{\varepsilon}_2)$. Combining it with eq. (38) yields the stress evolution equation

$$\dot{\sigma} + \frac{1}{\tau} (\sigma - \sigma_{\text{act}}) = G\dot{\varepsilon}, \quad (39)$$

where $\tau = \eta/G$ is the viscoelastic relaxation time. Equation (39) is the evolution equation of a classical Maxwell element modified by a constant shift in stress due to the active stress. This is reminiscent of the active force included in [38]. Note that the same equation also describes an active gel of polar filaments, as introduced in [103]. The active stress can of course be tensorial, for instance when the spatial distribution of motors is anisotropic. This can readily be taken into account by the formalism, here at tissue scale (analogous continuum descriptions have already been performed at the scale of the cytoskeleton [80]).

In the rheological diagram of fig. 7b, $\dot{\varepsilon}_{\text{act}}$ represents a constant deformation rate (counted negative when the tissue contracts). Such a rheological diagram has been introduced at the sub-cellular length scale, in the context of the actin-myosin cortex [104]; the active deformation rate $\dot{\varepsilon}_{\text{act}}$ is then interpreted in terms of the myosin concentration c_{my} , the step length l_{my} of the molecular motors and the binding rate τ_{my} , yielding: $\dot{\varepsilon}_{\text{act}} = -c_{\text{my}}l_{\text{my}}/\tau_{\text{my}}$.

Strikingly, the rheological diagram of fig. 7b leads to the same stress evolution equation as the diagram of fig. 7a. This can be directly checked by decomposing the total deformation rate as

$$\dot{\varepsilon} = \dot{\varepsilon}_1 + \dot{\varepsilon}_2 + \dot{\varepsilon}_{\text{act}} \quad (40)$$

and by defining the energy and dissipation functions again in the form of eqs. (3), (4) with $m = 1$

$$\mathcal{E}(\varepsilon, \varepsilon_1) = \frac{1}{2}G\varepsilon_1^2, \quad (41)$$

$$\mathcal{D}(\dot{\varepsilon}, \dot{\varepsilon}_1) = \frac{1}{2}\eta\dot{\varepsilon}_2^2 = \frac{1}{2}\eta(\dot{\varepsilon} - \dot{\varepsilon}_1 - \dot{\varepsilon}_{\text{act}})^2. \quad (42)$$

Injecting eqs. (41), (42) into eqs. (5), (6) and differentiating σ with respect to time yields

$$\dot{\sigma} + \frac{\sigma}{\tau} = G(\dot{\varepsilon} - \dot{\varepsilon}_{\text{act}}). \quad (43)$$

Equation (43) is the same as eq. (39) provided that σ_{act}/τ is replaced with $-G\dot{\varepsilon}_{\text{act}}$. Both rheological diagrams of fig. 7 are thus equivalent. This non-uniqueness also exists in rheological diagrams with only passive elements, see sect. 2.2.1.

3.4 Coupling non-mechanical fields to a rheological model

Suppose we need to describe an additional field which is non-mechanical and cannot be included in rheological diagrams. The dissipation function formalism, which allows

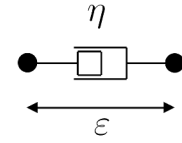


Fig. 8. Liquid of viscosity η .

to postulate forms of the energy and dissipation functions that respect the symmetries of the problem, provides a framework within which various couplings between fields may be introduced in a systematic manner.

A consistent continuum modelling of a cellular material sometimes requires to include tensors, for instance as variables of the energy and dissipation functions. Within a variational framework, Sonnet and coworkers [105,106] have performed a detailed study of the derivation of constitutive equations involving a tensorial order parameter. In epithelia, an example is given by noting that planar cell polarity proteins exhibit tissue scale ordered domains that are often best described by a tensor field [22,23].

Inspired by this last example, we treat the case of a viscous liquid (fig. 8), and choose to couple the deformation rate tensor $\dot{\varepsilon}$ to a second-order tensor Q in the dissipation function. We could have chosen a non-mechanical field which is scalar (appendix C.1), or vectorial: polar, for a usual oriented vector (appendix C.2), or axial, for a nematic-like vector. Of course, more complex couplings may be considered whenever needed, that also involve other ingredients such as tissue growth (sects. 3.2 and 4.2) or cell contractility (sect. 3.3).

Formally, eqs. (3), (4) should be written with an additional internal variable Q , so that $m = 1$, and with tensorial coupling parameters: $\mathcal{E} = \mathcal{E}(Q)$, $\mathcal{D} = \mathcal{D}(\dot{\varepsilon}, \dot{Q})$. Since trace and deviators of tensors have complementary symmetries, it is convenient to treat them as separate variables with distinct, scalar coupling parameters (see appendix B.2); equations (3), (4) thus read, with $m = 2$

$$\mathcal{E}(\text{dev } Q, \text{tr } Q) = \frac{\chi}{2} (\text{dev } Q)^2 + \frac{\bar{\chi}}{2} (\text{tr } Q)^2, \quad (44)$$

$$\begin{aligned} \mathcal{D}(\text{dev } \dot{\varepsilon}, \text{tr } \dot{\varepsilon}, \text{dev } \dot{Q}, \text{tr } \dot{Q}) \\ = \frac{\eta}{2} (\text{dev } \dot{\varepsilon})^2 + \frac{\bar{\eta}}{2} (\text{tr } \dot{\varepsilon})^2 + \frac{\xi}{2} (\text{dev } \dot{Q})^2 + \frac{\bar{\xi}}{2} (\text{tr } \dot{Q})^2 \\ + \delta \text{dev } \dot{\varepsilon} : \text{dev } \dot{Q} + \bar{\delta} \text{tr } \dot{\varepsilon} \text{tr } \dot{Q}, \end{aligned} \quad (45)$$

where the colon denotes the double contracted product between tensors: $a : b = \sum_{i,j} a_{ij}b_{ij}$. The parameters χ , $\bar{\chi}$, η , $\bar{\eta}$, ξ , $\bar{\xi}$ are non-negative and the inequalities $\delta^2 \leq \xi\eta$, $\bar{\delta}^2 \leq \bar{\xi}\bar{\eta}$ ensure the convexity of the dissipation function. From eq. (5) we first compute the stress tensor:

$$\text{dev } \sigma = \frac{\partial \mathcal{D}}{\partial \text{dev } \dot{\varepsilon}} = \eta \text{dev } \dot{\varepsilon} + \delta \text{dev } \dot{Q}, \quad (46)$$

$$\text{tr } \sigma = \frac{\partial \mathcal{D}}{\partial \text{tr } \dot{\varepsilon}} = \bar{\eta} \text{tr } \dot{\varepsilon} + \bar{\delta} \text{tr } \dot{Q}, \quad (47)$$

where a linear coupling to \dot{Q} modifies the usual constitutive equation of a viscous liquid. From eq. (6), we next

obtain the evolution equations

$$0 = \frac{\partial \mathcal{D}}{\partial \text{dev } \dot{Q}} + \frac{\partial \mathcal{E}}{\partial \text{dev } Q} = \xi \text{dev } \dot{Q} + \delta \text{dev } \dot{\epsilon} + \chi \text{dev } Q, \quad (48)$$

$$0 = \frac{\partial \mathcal{D}}{\partial \text{tr } \dot{Q}} + \frac{\partial \mathcal{E}}{\partial \text{tr } Q} = \bar{\xi} \text{tr } \dot{Q} + \bar{\delta} \text{tr } \dot{\epsilon} + \bar{\chi} \text{tr } Q, \quad (49)$$

which yield the evolution equations for the tensor Q :

$$\text{dev } \dot{Q} + \frac{\chi}{\xi} \text{dev } Q = -\frac{\delta}{\xi} \text{dev } \dot{\epsilon}, \quad (50)$$

$$\text{tr } \dot{Q} + \frac{\bar{\chi}}{\bar{\xi}} \text{tr } Q = -\frac{\bar{\delta}}{\bar{\xi}} \text{tr } \dot{\epsilon}. \quad (51)$$

Note that the relaxation times for the deviator and trace, respectively ξ/χ and $\bar{\xi}/\bar{\chi}$, can in principle be different. Inserting eqs. (50), (51) into eqs. (46), (47) yields the stress tensor

$$\text{dev } \sigma = \left(\eta - \frac{\delta^2}{\xi} \right) \text{dev } \dot{\epsilon} - \frac{\delta \chi}{\xi} \text{dev } Q, \quad (52)$$

$$\text{tr } \sigma = \left(\bar{\eta} - \frac{\bar{\delta}^2}{\bar{\xi}} \right) \text{tr } \dot{\epsilon} - \frac{\bar{\delta} \bar{\chi}}{\bar{\xi}} \text{tr } Q. \quad (53)$$

In the long time limit, the tensor Q tends to

$$\text{dev } Q \rightarrow -\frac{\delta}{\chi} \text{dev } \dot{\epsilon}, \quad (54)$$

$$\text{tr } Q \rightarrow -\frac{\bar{\delta}}{\bar{\chi}} \text{tr } \dot{\epsilon} \quad (55)$$

and the viscous stress tensor tends to

$$\text{dev } \sigma \rightarrow \eta \text{dev } \dot{\epsilon}, \quad (56)$$

$$\text{tr } \sigma \rightarrow \bar{\eta} \text{tr } \dot{\epsilon}. \quad (57)$$

As an example, the spatial distribution of a myosin (called Dachs) in the dorsal thorax of fruitfly pupae was studied quantitatively in [23]. Fluorescence microscopy images reveal a tissue scale organization of Dachs along lines, allowing to measure an orientation and an amplitude, from which a deviatoric tensor Q is defined. Dachs orientation correlates at the tissue scale with the direction of contraction quantified by the corresponding eigenvector of the velocity gradient tensor, as predicted by eq. (54).

3.5 Combining ingredients

The respective contributions of plasticity, growth and contractility to the rate of change in elastic deformation have been expressed by eqs. (15), (33), (40).

To model a given experiment, the relevant ingredients, for instance those listed in the introduction of sect. 3 or in fig. 5, can be assembled at will. Section 3.5.1 suggests how to classify them into intra- and inter-cell ingredients and sect. 3.5.2 presents an example of such a combination.

Table 1. Suggested contributions of various ingredients to the tissue volume and/or shape changes *via* intra-cell mechanisms (cell volume or shape) or inter-cell mechanisms (cell number and positions). Signs indicate positive and negative contributions. The contribution of contractility to cell volume, marked “(a)”, is discussed in sect. 3.5.1.

		Tissue volume		Tissue shape	
		intra	inter	intra	inter
		cell volume	cell number	cell shape	cell position
r_{sw}	cell swelling	+			
r_{apo}	apoptosis		-		
$\dot{\epsilon}_{\text{ck}}$	cytokinesis	-	+		+
$\dot{\epsilon}_{\text{act}}$	contractility	(a)		+	
$\dot{\epsilon}_{\text{p}}$	rearrangements				+

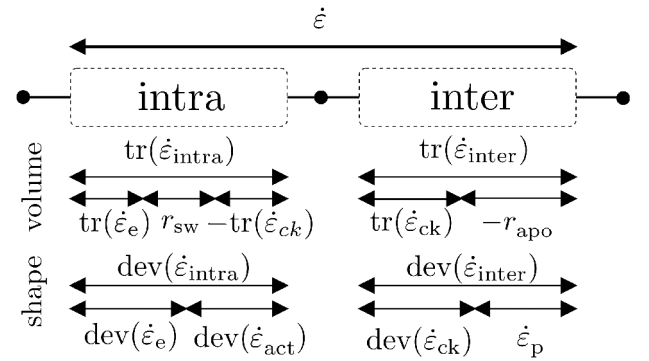


Fig. 9. Suggested decomposition of the tissue deformation, both volume (trace) and shape (deviatoric part), into contributions from various ingredients, acting at intra- or inter-cell levels.

3.5.1 Classification of ingredients

The distinction between “intra-cell” and “inter-cell” contributions can be complemented by a distinction between contributions which alter the shape and/or the volume of the tissue. Such distinction helps understanding the biological meaning of equations. For tensorial ingredients, eq. (9) becomes

$$\text{tr } \dot{\epsilon} = \text{tr } \dot{\epsilon}_{\text{intra}} + \text{tr } \dot{\epsilon}_{\text{inter}}, \quad (58)$$

$$\text{dev } \dot{\epsilon} = \text{dev } \dot{\epsilon}_{\text{intra}} + \text{dev } \dot{\epsilon}_{\text{inter}}. \quad (59)$$

This classification (table 1 and fig. 9) is merely indicative and should be adapted for any specific tissue under consideration according to the available knowledge or intuition. For instance, table 1 assumes (see (a)) that contractility does not change the actual volume of each cell, whether in a 3D tissue or in an epithelium, but that it may change the apparent surface area of cells in an epithelium.

Let us review some ingredients expected to contribute to the four parts of the total deformation rate tensor $\dot{\epsilon}$ (eqs. (58), (59)).

The rate of change in the cell volume can be written in terms of the isotropic elastic deformation, the cell swelling rate and the cytokinesis rate

$$\text{tr } \dot{\epsilon}_{\text{intra}} = \text{tr } \dot{\epsilon}_e + r_{\text{sw}} - \text{tr } \dot{\epsilon}_{\text{ck}}. \quad (60)$$

The number of cells increases due to cytokinesis and decreases due to apoptosis

$$\text{tr } \dot{\epsilon}_{\text{inter}} = \text{tr } \dot{\epsilon}_{\text{ck}} - r_{\text{apo}}. \quad (61)$$

The cell shape deformation rate can be expressed in terms of the deviatoric elastic deformation, and the active contractility rate

$$\text{dev } \dot{\epsilon}_{\text{intra}} = \text{dev } \dot{\epsilon}_e + \text{dev } \dot{\epsilon}_{\text{act}}. \quad (62)$$

Finally, the arrangement of cell positions is affected by cytokinesis and by the cell rearrangement contribution to plasticity, which is purely deviatoric

$$\text{dev } \dot{\epsilon}_{\text{inter}} = \text{dev } \dot{\epsilon}_{\text{ck}} + \dot{\epsilon}_{\text{p}}. \quad (63)$$

Each ingredient listed above then provides a term either in the energy \mathcal{E} or in the dissipation function \mathcal{D} , except motor elements (sects. 3.2.3 and 3.3) which correspond to $\dot{\epsilon}_{\text{act}} = \text{const}$.

Within the dissipation function framework (sect. 2.2.3), eqs. (58)-(63) play the role of the topological relations between deformation rate variables, see eq. (16). Combined together, eqs. (58)-(63) enable to split the evolution of the elastic deformation (eq. (33)) into the following two equations:

$$\text{tr } \dot{\epsilon}_e = \text{tr } \dot{\epsilon} - r_{\text{sw}} + r_{\text{apo}}, \quad (64)$$

$$\text{dev } \dot{\epsilon}_e = \text{dev } \dot{\epsilon} - \text{dev } \dot{\epsilon}_{\text{act}} - \text{dev } \dot{\epsilon}_{\text{ck}} - \dot{\epsilon}_{\text{p}}. \quad (65)$$

3.5.2 A complex example

To open the way towards more realistic, complex descriptions, we now present an example of a tissue rheology model that incorporates most ingredients listed in the introductions of sects. 3 and 3.5. Figure 10 is decomposed into four blocks. The upper line corresponds to the deviatoric part of the deformation, and the lower to the volume-related rheology. Each part is further decomposed into intra-cell rheology (left block) and inter-cell processes (right block).

Figure 10 indicates the topology of the diagram, and the numerous parameters involved: G_1 , G_2 , η_{cyto} , σ_Y , η_3 , $\text{dev } \dot{\epsilon}_{\text{ck}}$, r_{sw} , η_{sw} , $\text{tr } \dot{\epsilon}_{\text{ck}}$, η_{apo} , r_{apo} . It yields the energy and dissipation functions

$$\mathcal{E} = G_1(\text{dev } \epsilon_1)^2 + G_2(\text{dev } \epsilon_{\text{intra}})^2, \quad (66)$$

$$\begin{aligned} \mathcal{D} = & \eta_{\text{cyto}}(\text{dev } \dot{\epsilon}_{\text{intra}} - \text{dev } \dot{\epsilon}_1)^2 \\ & + \sigma_Y |\text{dev } \dot{\epsilon} - \text{dev } \dot{\epsilon}_{\text{intra}} - \text{dev } \dot{\epsilon}_3 - \text{dev } \dot{\epsilon}_{\text{ck}}| \\ & + \eta_3(\text{dev } \dot{\epsilon}_3)^2 + \frac{1}{2}\eta_{\text{sw}}(\text{tr } \dot{\epsilon}_{\text{intra}} - r_{\text{sw}} + \text{tr } \dot{\epsilon}_{\text{ck}})^2 \\ & + \frac{1}{2}\eta_{\text{apo}}(\text{tr } \dot{\epsilon} - \text{tr } \dot{\epsilon}_{\text{intra}} - \text{tr } \dot{\epsilon}_{\text{ck}} + r_{\text{apo}})^2, \end{aligned} \quad (67)$$

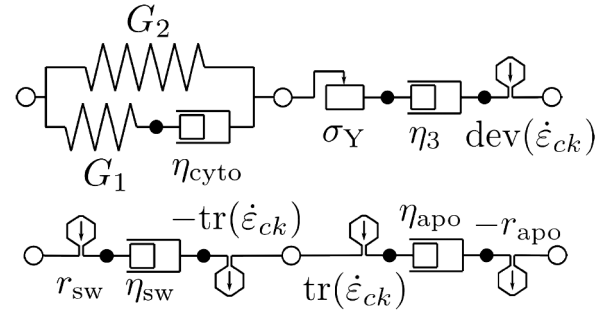


Fig. 10. Model of tissue rheology using ingredients listed in sect. 3. The upper line corresponds to shape (deviatoric contributions) and the lower line to volume (trace contributions). Intra-cell (left) and inter-cell (right) contributions are separated by large open circles. Arrows within hexagons symbolize the sign of contributions to strain rates.

where the following independent variables have been chosen (see sect. 2.2.3 and appendix B.1): $\text{dev } \epsilon_1$ and $\text{dev } \epsilon_{\text{intra}}$ for the springs, $\text{dev } \dot{\epsilon}_3$ for the dashpot η_3 , $\text{tr } \epsilon_{\text{intra}}$ for the cell volume, and as usual $\text{dev } \dot{\epsilon}$ and $\text{tr } \dot{\epsilon}$ for the total deformation rate.

The problem can then be treated according to the method detailed in appendix B.2 to obtain a set of equations describing the behaviour of the tissue. For this example, the case of large deformations is treated in appendix D.2.4.

4 Applications to the mechanics of cell aggregates

In the present Section, we combine ingredients introduced in sect. 3 to write and solve the dynamical equations in two more realistic examples. These examples are inspired by the rheology of cellular aggregates, first when deformed on a timescale short compared to the typical cell cycle time r_{cc}^{-1} (sect. 4.1), second when growing between fixed walls on a timescale long compared to r_{cc}^{-1} (sects. 4.2 and 4.3). In both cases, we separate the contributions of intra- and inter-cellular processes to aggregate rheology. Both examples derive from a rheological diagram, but more complex situations, including for instance non-mechanical fields as in sect. 3.4, can be solved within the same formalism.

4.1 Without divisions: creep response

Although an actual cell aggregate is complex, we crudely model it by combining an intra-cellular viscoelasticity and an inter-cellular plasticity (fig. 11): one aim of the present section is to illustrate their interplay. For simplicity, we neglect aggregate volume changes, and use scalar variables; we defer a tensorial treatment to sect. 4.2.

Each cell is modelled as a fixed amount of viscous liquid enclosed in an elastic membrane which prevents it from flowing indefinitely at long times. We thus model the cell

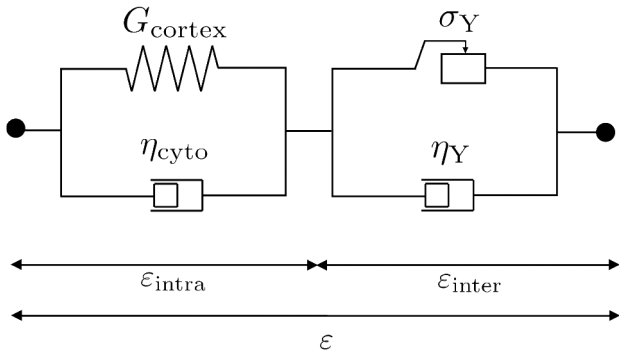


Fig. 11. Example of rheological diagram for a cell aggregate in the absence of growth. The intra-cellular rheology (left) is viscoelastic, the inter-cellular one (right) is viscoplastic.

as a viscoelastic *solid*, more precisely a Kelvin-Voigt element: a spring which reflects the effective cell shear elastic modulus G_{cortex} (typically of order of the cell cortex tension divided by the cell size) is in parallel with a dashpot which reflects the cytoplasm viscosity η_{cyto} .

Cells need to undergo a finite deformation before triggering a rearrangement. When the stress exerted on the aggregate exceeds the yield stress σ_Y , cells rearrange; the aggregate flows like a liquid with a viscosity η_Y much larger than η_{cyto} [11]. If the aggregate presents a high level of active cell contour fluctuations, whatever their origin, the cells undergo rearrangements more easily: in practice, this biological activity will lower the yield stress σ_Y and the viscosity η_Y [10].

For simplicity, we turn to a one-dimensional description, and assume that $\varepsilon = \varepsilon_{\text{intra}} + \varepsilon_{\text{inter}}$. Their time-derivatives $\dot{\varepsilon}_{\text{inter}}$ and $\dot{\varepsilon}_{\text{intra}}$ correspond to the respective 1D projections of the plastic deformation rate $\dot{\varepsilon}_p$ and of the elastic deformation rate $\dot{\varepsilon}_e$.

From fig. 11, the energy and dissipation functions of the independent variables ε and $\varepsilon_{\text{intra}}$ read:

$$\mathcal{E}(\varepsilon, \varepsilon_{\text{intra}}) = \frac{1}{2} G_{\text{cortex}} \varepsilon_{\text{intra}}^2, \quad (68)$$

$$\mathcal{D}(\dot{\varepsilon}, \dot{\varepsilon}_{\text{intra}}) = \frac{1}{2} \eta_{\text{cyto}} \dot{\varepsilon}_{\text{intra}}^2 + \frac{1}{2} \eta_Y (\dot{\varepsilon} - \dot{\varepsilon}_{\text{intra}})^2 + \sigma_Y |\dot{\varepsilon} - \dot{\varepsilon}_{\text{intra}}|, \quad (69)$$

where $\dot{\varepsilon} - \dot{\varepsilon}_{\text{intra}} = \dot{\varepsilon}_{\text{inter}}$ vanishes when $|\sigma| < \sigma_Y$. From eqs. (5), (6) we obtain:

$$\begin{aligned} \sigma &= \frac{\partial \mathcal{D}}{\partial \dot{\varepsilon}} + \frac{\partial \mathcal{E}}{\partial \varepsilon} \\ &= \eta_Y (\dot{\varepsilon} - \dot{\varepsilon}_{\text{intra}}) + \sigma_Y \frac{\dot{\varepsilon} - \dot{\varepsilon}_{\text{intra}}}{|\dot{\varepsilon} - \dot{\varepsilon}_{\text{intra}}|}, \end{aligned} \quad (70)$$

$$\begin{aligned} 0 &= \frac{\partial \mathcal{D}}{\partial \dot{\varepsilon}_{\text{intra}}} + \frac{\partial \mathcal{E}}{\partial \varepsilon_{\text{intra}}} \\ &= G_{\text{cortex}} \varepsilon_{\text{intra}} + \eta_{\text{cyto}} \dot{\varepsilon}_{\text{intra}} \\ &\quad - \eta_Y (\dot{\varepsilon} - \dot{\varepsilon}_{\text{intra}}) - \sigma_Y \frac{\dot{\varepsilon} - \dot{\varepsilon}_{\text{intra}}}{|\dot{\varepsilon} - \dot{\varepsilon}_{\text{intra}}|}. \end{aligned} \quad (71)$$

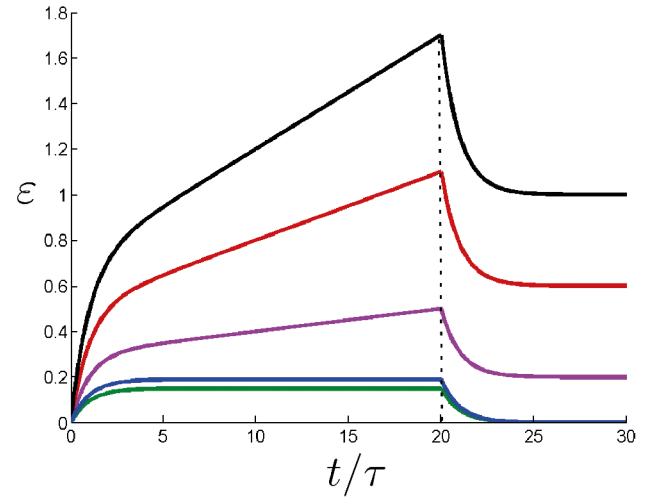


Fig. 12. Creep curves. A constant stress σ is applied from time $t = 0$ to $T_{\text{stop}} = 20\tau$ (vertical dashed line), where $\tau = \eta_{\text{cyto}}/G_{\text{cortex}}$ is the viscoelastic time. The deformation ε is plotted during a transient increase, then a decrease. From bottom to top, $\sigma/\sigma_Y = 0.6$ (green), 0.95 (blue), 1.5 (violet), 2.5 (red), 3.5 (black), where σ_Y is the yield stress

We can now turn to predictions. For instance, in a “creep experiment”, the total stress is zero until $t = 0$, then is set at a constant value σ during the time interval from $t = 0$ to $t = T_{\text{stop}}$. Figure 12 represents the corresponding creep curves, *i.e.* the time evolution of the total deformation ε , obtained as the analytical solution of eqs. (70), (71).

If the magnitude of the applied stress σ is lower than the yield stress σ_Y , the deformation ε reaches a plateau value equal to σ/G_{cortex} . When σ is brought back to zero, the deformation ε relaxes back to zero over a time $\tau = \eta_{\text{cyto}}/G_{\text{cortex}}$: this viscoelastic time τ is a natural timescale of the material and reflects the individual cell rheology.

If σ is larger than the yield stress σ_Y , after a typical time τ cell shapes reach their maximal deformation, so that the aggregate thereafter flows only as a result of cell rearrangements: the aggregate deformation ε increases steadily at a rate σ/η_Y . When σ is brought back to zero, the cell shapes relax to equilibrium within a time τ . The total deformation ε correspondingly relaxes, yet not back to zero.

The creep curves shown in fig. 12 are similar to quantitative measurements performed during the micropipette aspiration of cell aggregates which were assumed to be viscoelastic [63]. A similar yield behavior was observed when stretching a suspended cell monolayer: the monolayer deformation reached a plateau at low applied stress, while a creep behavior appeared at higher stress [39]. The authors observe no divisions or rearrangements in the course of deformations that reach circa 70%, which suggests that in their experiment, the creep behavior arises from an intra-cell contribution.

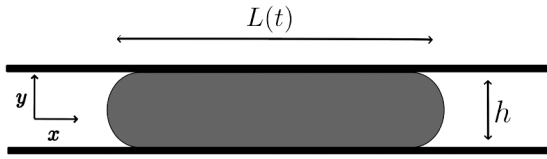


Fig. 13. Sketch of a cell aggregate confined between parallel plates [107], a distance h apart. The size L increases with time due to cell division cycles.

4.2 With divisions: inhomogeneous proliferation

When the duration of the experiment becomes much longer than r_{cc}^{-1} , cell divisions must be taken into account and the aggregate flows even under a weak stress [9].

Figure 13 represents an experiment [107] where a cell aggregate is confined between parallel rigid plates. The aggregate length $L(t)$ grows from initially $L_0 \sim 400 \mu\text{m}$ to $L_T \sim 700 \mu\text{m}$ in $T = 3$ days and $L_T \sim 1200 \mu\text{m}$ in $T = 6$ days. We thus estimate the growth rate as $\alpha_g \approx 2 \log(L_T/L_0)/T \simeq 4.2 \cdot 10^{-6} \text{s}^{-1}$, where the factor 2 reflects the fact that growth occurs effectively in only two dimensions: cells divide mostly at the aggregate periphery. The main hypothesis proposed by [107] is that the stress induced by growth in the confined aggregate could mechanically inhibit mitosis.

4.2.1 Model with divisions

We propose to qualitatively model the aggregate growth coupled to its mechanical response (determined in sect. 4.1). Assuming translational invariance along z , we treat this problem in the xy plane ($d = 2$). We introduce separate rheological diagrams for the trace and the deviator.

According to the mass conservation (eq. (24)), the trace $\text{tr} \dot{\epsilon}$ of the deformation rate is equal to the growth rate α_g of the aggregate. Within a linear approximation [12], we assume that α_g decreases with the pressure $P = -\text{tr} \sigma/d$, from its value $\dot{\epsilon}_g$ at zero pressure, as

$$\alpha_g = \dot{\epsilon}_g \left(1 + \frac{\text{tr} \sigma}{P_g d} \right), \quad (72)$$

where we use the pressure P_g actively generated by the aggregate at zero deformation rate, *e.g.* when confined between fixed walls. We deduce the rheological equation for the trace (fig. 14, top part)

$$\text{tr} \dot{\epsilon} = \dot{\epsilon}_g + \frac{\text{tr} \sigma}{\eta_g}, \quad (73)$$

where we define an effective growth-induced viscosity coefficient η_g [12]

$$\eta_g = \frac{P_g d}{\dot{\epsilon}_g}, \quad (74)$$

which differs from the effective division-induced viscosity coefficient

$$\eta_{cc} = \frac{G}{r_{cc}}, \quad (75)$$

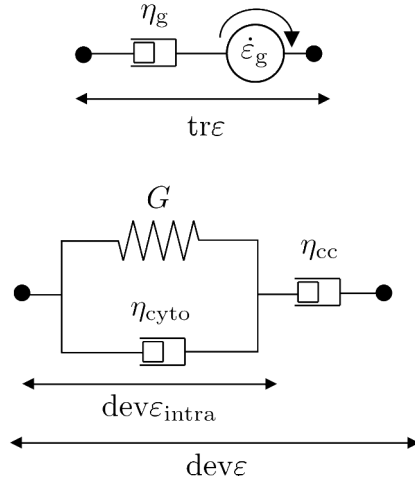


Fig. 14. Rheological diagrams for the trace (top) and the deviator (bottom) of the stress in a cell aggregate in the presence of growth. Here $\dot{\epsilon}_g$ is the aggregate growth rate at zero pressure and η_g quantifies the influence of pressure on aggregate growth (eq. (74)), G is the effective cell shear elastic modulus, η_{cyto} the single cell viscosity, η_{cc} the aggregate viscosity related to divisions.

where r_{cc} is the division rate.

We further assume that deviatoric stresses generated by the growth are lower than the yield stress σ_Y . On the other hand, here (as opposed to sect. 4.1), we consider time scales which are long enough (compared with the cell division cycle) that the aggregate viscosity η_{cc} related to cell divisions is now relevant. The inter-cellular viscoplastic element of fig. 11 is replaced by a dashpot (fig. 14, bottom).

The energy and dissipation functions for these diagrams read

$$\mathcal{E}(\text{dev} \epsilon_{\text{intra}}) = \frac{1}{2} G (\text{dev} \epsilon_{\text{intra}})^2, \quad (76)$$

$$\mathcal{D}(\text{tr} \dot{\epsilon}, \text{dev} \dot{\epsilon}, \text{dev} \dot{\epsilon}_{\text{intra}}) = \frac{1}{2} \eta_g (\text{tr} \dot{\epsilon} - \dot{\epsilon}_g)^2 + \frac{1}{2} \eta_{cyto} (\text{dev} \dot{\epsilon}_{\text{intra}})^2 + \frac{1}{2} \eta_{cc} (\text{dev} \dot{\epsilon} - \text{dev} \dot{\epsilon}_{\text{intra}})^2. \quad (77)$$

Considering $\text{dev} \epsilon_{\text{intra}}$, $\text{tr} \dot{\epsilon}$, $\text{dev} \dot{\epsilon}$ and $\text{dev} \dot{\epsilon}_{\text{intra}}$ as independent variables and using eqs. (B.10)-(B.13), eqs. (76), (77) yield

$$\text{tr} \sigma = \eta_g (\text{tr} \dot{\epsilon} - \dot{\epsilon}_g), \quad (78)$$

$$\text{dev} \sigma = \eta_{cc} (\text{dev} \dot{\epsilon} - \text{dev} \dot{\epsilon}_{\text{intra}}), \quad (79)$$

$$0 = G \text{dev} \epsilon_{\text{intra}} + \eta_{cyto} \text{dev} \dot{\epsilon}_{\text{intra}} + \eta_{cc} (\text{dev} \dot{\epsilon}_{\text{intra}} - \text{dev} \dot{\epsilon}). \quad (80)$$

Finally, using a few substitutions to eliminate $\text{dev} \epsilon_{\text{intra}}$ and $\text{dev} \dot{\epsilon}_{\text{intra}}$ between eqs. (79)-(80), we obtain

$$\left(1 + \frac{\eta_{cyto}}{\eta_{cc}} \right) \text{dev} \dot{\sigma} + \frac{\text{dev} \sigma}{\tau_{cc}} = \eta_{cyto} \text{dev} \ddot{\epsilon} + G \text{dev} \dot{\epsilon}, \quad (81)$$

where $\tau_{cc} \approx \eta_{cc}/G = r_{cc}^{-1}$ is a viscoelastic relaxation time associated with cell division cycles.

Provided gravity and other body forces are negligible, the stress is divergence-free in the bulk of the aggregate

$$\partial_x \sigma_{xx} + \partial_y \sigma_{xy} = 0, \quad (82)$$

$$\partial_y \sigma_{yy} + \partial_x \sigma_{xy} = 0. \quad (83)$$

4.2.2 Symmetries

Equations (78)-(83) can be simplified as follows. We assume (and check *a posteriori*) that internal forces are much larger than inertial terms in eq. (13), which thus reduces to eq. (14). Furthermore, the plates are rigid and immobile: we can safely assume that the vertical component v_y of the velocity is equal to zero not only at the plates, but also in the whole aggregate (that condition is possibly violated within a small edge region, of width comparable to the thickness h). As a consequence, the vertical component of the deformation rate, $\dot{\epsilon}_{yy}$, is identically zero.

Further simplifications result from the symmetry of the aggregate both in direction x along the length and in direction y across the thickness. Some quantities are even functions of the y -coordinate, namely the horizontal velocity v_x and the horizontal component $\dot{\epsilon}_{xx}$ of the deformation rate, stress components σ_{xx} and σ_{yy} aligned with the plates, and y -derivatives of odd functions, such as $\partial_y \sigma_{xy}$. Other quantities are odd functions of y , for instance shear components of the stress σ_{xy} and of the deformation rate $\dot{\epsilon}_{xy}$, x -derivatives of other odd functions such as $\partial_x \sigma_{xy}$, and y -derivatives of even functions such as $\partial_y v_x$ or $\partial_y \sigma_{yy}$.

As a result, after averaging along y , the deformation rate has only one non-zero component $\dot{\epsilon}_{xx}$; the deviatoric stress has only diagonal terms and thus only one independent component, say $(\sigma_{xx} - \sigma_{yy})/2$.

With these simplifications, eqs. (78)-(82) become

$$\sigma_{xx} + \sigma_{yy} = \eta_g (\dot{\epsilon}_{xx} - \dot{\epsilon}_g), \quad (84)$$

$$\left(1 + \frac{\eta_{\text{cyto}}}{\eta_{\text{cc}}}\right) (\dot{\sigma}_{xx} - \dot{\sigma}_{yy}) + \frac{\sigma_{xx} - \sigma_{yy}}{\tau_{\text{cc}}} = \eta_{\text{cyto}} \ddot{\epsilon}_{xx} + G \dot{\epsilon}_{xx}, \quad (85)$$

$$\partial_x \sigma_{xx} = -\frac{2}{h} \sigma_{xy}|_{y=h/2}. \quad (86)$$

We now assume that $\eta_{\text{cyto}} \ll \eta_{\text{cc}} \ll \eta_g$, based on the following orders of magnitude. Single cell viscosity η_{cyto} is around 10^2 Pa s [108]. Aggregate viscosity η_{cc} extracted from cell aggregates fusion and aspiration is around 10^5 Pa s [63,109]. Using data of cell aggregate growth under pressure [12], a value of η_g around 10^9 Pa s has been proposed [110]. Encapsulated growing aggregates which deform a capsule yield a value $P_g \sim 2000$ Pa [43], where a dramatic decrease of the aggregate growth is observed. Taking $\dot{\epsilon}_g \sim 5 \cdot 10^{-6} \text{ s}^{-1}$ yields η_g around 10^9 Pa s, consistent with the previous estimation.

4.2.3 Boundary conditions

Equations (84)-(86) must be complemented with the free edge boundary condition

$$\sigma_{xx}|_{x=\pm L/2} = 0. \quad (87)$$

Let us first assume that we could neglect the friction of horizontal plates, $\sigma_{xy}|_{y=\pm h/2} = 0$. Then eq. (86) and the edge boundary condition (eq. (87)) would imply a vanishing horizontal stress in the whole aggregate: $\sigma_{xx}(x) = 0$. Under these conditions, eqs. (84)-(85) would predict that after a transient time of order τ_{cc} , the vertical stress and the horizontal deformation rate would reach a stationary value: $\sigma_{yy} \rightarrow -\eta_{\text{cc}} \dot{\epsilon}_g$ and $\dot{\epsilon}_{xx} \rightarrow \dot{\epsilon}_g$. Hence, an exponential increase of the aggregate size $L(t) \sim \exp(\dot{\epsilon}_g t)$ would be expected, with a spatially uniform proliferation, at odds with the experimental observation that cells divide only at the aggregate periphery.

This is why we do explicitly take into account the friction on plates. In a linear approximation, the friction can be assumed proportional to the local aggregate velocity

$$\sigma_{xy} \left(x, \frac{h}{2}\right) = -\zeta v_x \left(x, \frac{h}{2}\right). \quad (88)$$

Under the assumption $\eta_{\text{cyto}} \ll \eta_{\text{cc}}$, eq. (81) implies $\sigma_{xy} \simeq \eta_{\text{cc}} \partial_y v_x$. Hence, if we assume that the friction coefficient ζ is small enough that we can neglect the velocity variations across the aggregate thickness $|h \partial_y v_x / v_x| \simeq h \zeta / \eta_{\text{cc}}$, the velocity profile is approximately a plug flow: $v_x(x, h/2) \simeq v_x(x)$. Combining eqs. (86), (88) and the relation $\dot{\epsilon}_{xx} = \partial_x v_x$ (eq. (11)), yields

$$v_x = \frac{h}{2\zeta} \partial_x \sigma_{xx}, \quad (89)$$

$$\dot{\epsilon}_{xx} = \frac{h}{2\zeta} \partial_x^2 \sigma_{xx}. \quad (90)$$

Within the approximation $\eta_{\text{cyto}} \ll \eta_{\text{cc}} \ll \eta_g$, combining eqs. (84), (85), (90) so as to eliminate σ_{yy} yields an evolution equation for the horizontal component of the stress

$$\tau_{\text{cc}} \dot{\sigma}_{xx} + \sigma_{xx} = -P_g + \tau_{\text{cc}} \lambda^2 \partial_x^2 \dot{\sigma}_{xx} + \lambda^2 \partial_x^2 \sigma_{xx},$$

where the characteristic length λ is

$$\lambda = \sqrt{\frac{\eta_g h}{4\zeta}}, \quad (91)$$

while σ_{yy} passively follows σ_{xx} according to

$$\sigma_{yy} = -\sigma_{xx} + 2\lambda^2 \partial_x^2 \sigma_{xx} - 2P_g. \quad (92)$$

The motion of the aggregate edge results from the velocity: $\frac{1}{2} \dot{L}(t) = v_x(L/2, t)$. From eqs. (87), (89), the boundary conditions are

$$\sigma_{xx} \left(-\frac{L}{2}, t\right) = \sigma_{xx} \left(\frac{L}{2}, t\right) = 0, \quad (93)$$

$$\frac{h}{\zeta} \partial_x \sigma_{xx} \left(\frac{L}{2}\right) = \dot{L}. \quad (94)$$

4.3 Resolution

4.3.1 Change of variables

We introduce the rescaled variables $X = \frac{2x}{L(t)}$, $\Sigma(X, t) = \sigma_{xx}(x, t)$, $\Lambda(t) = \frac{2\lambda}{L(t)}$ and the new function

$$F(X, t) = \Sigma - \Lambda^2(t) \partial_X^2 \Sigma + P_g. \quad (95)$$

Equation (91) becomes

$$\tau_{cc} \partial_t F + F = \frac{\tau_{cc} X \dot{L}(t)}{L(t)} \partial_X F. \quad (96)$$

The boundary conditions (eqs. (93), (94)) read:

$$\Sigma_{xx}(-1, t) = \Sigma_{xx}(1, t) = 0, \quad (97)$$

$$\frac{2h}{\zeta L(t)} \partial_X \Sigma_{xx}(1, t) = \dot{L}. \quad (98)$$

Equation (96) can be further rewritten in terms of the variable $Z = \log X$ and the function $K(Z, t) = \exp(t/\tau_{cc})F(X, t)$

$$\partial_t K(Z, t) - \frac{\dot{L}(t)}{L(t)} \partial_Z K(Z, t) = 0. \quad (99)$$

4.3.2 Initial conditions

Just before the first time of contact between the aggregate and the walls, the cells constituting the aggregate do not undergo any elastic deformation. Thus $\text{dev } \varepsilon_{\text{intra}}(t = 0^-) = 0$. The cell deformation is continuous in time, so $\text{dev } \varepsilon_{\text{intra}}(t = 0^+) = 0$. From this condition and eq. (80), we obtain:

$$\text{dev } \dot{\varepsilon}_{\text{intra}}(x, 0^+) = \frac{\eta_{cc}}{\eta_{cc} + \eta_{\text{cyto}}} \text{dev } \dot{\varepsilon}(x, 0^+). \quad (100)$$

Substituting eq. (100) into eq. (79), and eliminating σ_{yy} with eq. (78), we obtain

$$2\sigma_{xx}(x, 0^+) = \left(\eta_g + \frac{\eta_{cc}\eta_{\text{cyto}}}{\eta_{cc} + \eta_{\text{cyto}}} \right) \dot{\varepsilon}_{xx}(x, 0^+) - \eta_g \dot{\varepsilon}_g. \quad (101)$$

Using again $\eta_{\text{cyto}} \ll \eta_{cc} \ll \eta_g$ and eq. (90), we obtain

$$\sigma_{xx}(x, 0^+) - \lambda^2 \partial_x^2 \sigma_{xx}(x, 0^+) = -P_g. \quad (102)$$

4.3.3 Analytical solution

Solving eq. (99) with the boundary conditions of eqs. (97), (98) and the initial condition of eq. (102) yields the following analytical solution, in terms of the initial variables:

$$\frac{L}{2\lambda} = \sinh^{-1} \left(e^{\dot{\varepsilon}_g t} \sinh \frac{L_0}{2\lambda} \right), \quad (103)$$

$$\sigma_{xx} = P_g \left[\frac{\cosh \frac{x}{\lambda}}{\cosh \frac{L(t)}{2\lambda}} - 1 \right]. \quad (104)$$

Equation (89) then yields

$$v_x \left(\frac{L}{2}, t \right) = \frac{h P_g}{2\zeta \lambda} \tanh \frac{L}{2\lambda}, \quad (105)$$

while eq. (92) yields

$$\sigma_{yy} = \sigma_{xx} \quad (106)$$

and from eqs. (104), (106), the pressure is

$$P = -\frac{\sigma_{xx} + \sigma_{yy}}{2} = P_g \left[1 - \frac{\cosh \frac{x}{\lambda}}{\cosh \frac{L(t)}{2\lambda}} \right]. \quad (107)$$

4.3.4 Discussion

Equation (103) shows that as long as $L(t) \ll 2\lambda$, the aggregate growth rate is $\dot{L}(t) \approx \dot{\varepsilon}_g L(t)$. The aggregate length increases with time as $L(t) \approx L(0) \exp(\dot{\varepsilon}_g t)$, as it would be in the absence of friction (sect. 4.2.3).

For $L(t) \gg 2\lambda$, the aggregate growth rate is $\dot{L}(t) \approx 2\dot{\varepsilon}_g \lambda$. The aggregate grows linearly in time as $L(t) \approx 2\dot{\varepsilon}_g \lambda t$. The growth is localized in a zone of typical size λ at the border of the aggregate. After a transient regime which lasts of the order of τ_{cc} , the pressure decreases exponentially on a lengthscale λ from 0 at the border of the aggregate to P_g inside the aggregate.

Since cell division can be affected by mechanical stresses, this model could explain why cell divisions are inhibited inside the confined growing aggregate, except in a region of width λ [107]. Since the pressure affects the growth rate, which in turn affects η_{cc} , the model could be extended to include the spatial variation of η_{cc} : the pressure would be expected to increase dramatically in the inner part of the aggregate.

The length λ defined in eq. (91) increases as the square root of h : this could be checked experimentally by changing h . The pressure profile predicted by eq. (107), plotted in fig. 15, could be checked by looking at aggregates growing between deformable plates.

We can estimate *a posteriori* orders of magnitude in experiments [107]. From the width of the proliferating region, we estimate λ to be of order of 10^{-4} m. Velocities are of order $\frac{1}{2}\alpha_g L$, *i.e.* a few 10^{-10} ms^{-1} . Based on a typical value of the effective viscosity $\eta_g \sim 10^9$ Pa s [12] and the growth rate α_g , the stationary value of pressure P_g in the aggregate is estimated as a few 10^3 Pa. The inertial terms in eq. (13) are respectively $\rho \partial_t v \sim \rho v/T$ and $\rho v \nabla v \sim \rho v^2/\lambda$, both of order of a few 10^{-13} N m^{-3} : they are much smaller than the other terms, for instance the divergence of the stress $\nabla \cdot \sigma$ which is of order of P_g/λ , namely a few 10^7 N m^{-3} .

When confining plates are removed, the aggregate shape relaxes first quickly, then more slowly towards a sphere [10, 107]. The fast relaxation is over the time scale of minutes whereas the slower one is over many hours. The

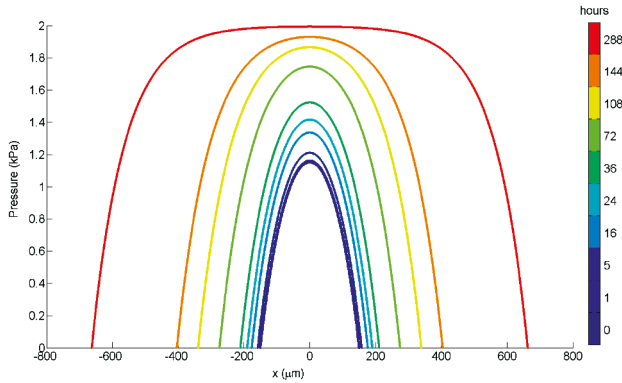


Fig. 15. Space dependence of the pressure in the confined growing aggregate, at different times (eq. (107)). Parameters (see text): $\tau_{cc} = 8$ h, $\lambda = 100 \mu\text{m}$, $\dot{\epsilon}_g = 5.10^{-6} \text{s}^{-1}$, $P_g = 2000$ Pa.

fast relaxation could correspond to the relaxation of the elastic deformation of individual cells generated by confined growth, where the driving force is dominated by the cell elasticity rather than surface tension, and the dissipation dominated by the intra-cellular viscosity. Conversely, the slow relaxation phase could correspond to the rounding of the aggregate under surface tension after the relaxation of stored elasticity. Measuring the relaxation amplitude as a function of the position in the aggregate could be a way to estimate the spatial profile of the deviatoric stress generated by growth.

5 Conclusion

When modelling the mechanical behaviour of living tissues, it is important to be able to build a sensible rheological model and to derive the corresponding dynamical equations in a systematic manner. We present here a toolbox to model the mechanics underlying the morphogenesis of tissues whose mechanical behaviour is that of a continuous material. Once a given problem has been analysed in details and appropriately simplified, this toolbox should enable to incorporate into models large amounts of data regarding feedbacks between genetics and mechanics.

We have suggested to proceed in four steps. First, to list the relevant ingredients, classified into intra-cell mechanisms (cell elasticity and relaxation, cell growth, cell contractility) and inter-cell mechanisms (rearrangements, division and apoptosis), which affect the tissue shape and/or volume. Second, to combine the mechanical ingredients into rheological diagrams. Third, to translate such diagrams into the dissipation function formalism, taking into account couplings with non-mechanical fields. Fourth, to derive a set of partial differential equations to be solved.

Section 5.1 discusses the dissipation function formalism. Section 5.2 examines possible applications. Section 5.3 opens perspectives.

5.1 Dissipation function formalism

The dissipation function formalism has the following limitations. It can include only a subclass of all conceivable mechanical or biological ingredients. It obeys the Onsager symmetry theorem only when fluxes and forces behave similarly under time reversal.

Conversely, the dissipation function formalism has the following advantages. It is a convenient tool for building complex models and obtaining in an automatic way the full set of partial differential equations which respect tensorial symmetry in any dimensions. It includes and generalizes the rheological diagram formalism and the hydrodynamic formalism. For tissues with non-mechanical ingredients, it allows to systematically explore possible couplings. Its coupling coefficients arise as cross partial derivatives, thus derive from a smaller number of free parameters than in the hydrodynamics formalism. It is suitable for nonlinear terms, whether analytic or not, including terms dominant over linear terms, like plasticity. In the case of small deformations, the convexity of the energy and dissipation functions warrants that there exists a unique solution, and that it satisfies the second law of thermodynamics. Numerically, it allows to use a variational approach, which makes it useful for the resolution of the dynamical equations. In view of these advantages, we recommend to adopt the dissipation function formalism for models of living tissues within continuum material mechanics.

A complete set of partial differential equations modelling the tissue can be explicitly derived from the energy and dissipation functions, using the method described in sect. 2.2.3 and appendix B, and can be solved numerically. Ingredients specific to living tissues, such as cell contractility or growth, can be included in a consistent manner as shown in sect. 3, which includes both simple and complex examples. An example is fully solved in sect. 4.

5.2 Practical applications

Tools exist to analyse 2D or 3D movies of tissue dynamics and perform quantitative measurements within a continuum mechanics description. Data can be compared with the model predictions, *i.e.* numerical solutions of the model equations. Such a comparison is instrumental in determining the values of the unknown parameters, and is indeed already possible on a large scale in both animal and vegetal tissues.

To constrain the models, it is essential to limit the number of mechanical parameters, which should be much lower than the number of measurements available. In this respect, the continuum description is more economical than a simulation of a whole tissue at the cell scale. This advantage may be crucial when, *e.g.*, studying feedbacks between gene expression and mechanical response. *In situ* measurements of local force and stress are improving at a quick pace and will hopefully be soon compared with local elastic deformation measurements. Our modelling approach should help exploit the future wealth of available data and incorporate it into a consistent picture.

In principle, the present approach should be relevant to dynamically evolving assemblies of cohesive cells such as encountered in animal tissues during development, wound healing, tumorigenesis, as well as in *in vitro* aggregates. In other types of tissues, we expect some of the present ingredients to be irrelevant. In an adult tissue without any significant chemical or mechanical stress, cell division and rearrangements can become negligible. In a tissue where cell divisions and apoptoses are negligible and where a strong cell-cell adhesion or an extra-cellular matrix hinders plasticity, we expect the tissue rheology to essentially reflect the single cell behaviour. The present approach should thus remain relevant, provided some of the parameters are taken as zero.

5.3 Perspectives

Different issues need to be overcome in order to validate continuum descriptions of tissues from experimental data. First, an adequate averaging procedure should be chosen. An optimal length scale of measurement must be properly defined, larger than the typical cell size, but smaller than the sample size, and therefore suitable for hydrodynamics. Averages over time or over an ensemble of experiments performed in identical conditions may improve the signal-to-noise ratio. A second difficulty originates in the large size of data, in terms of manipulation and representation. Third, the formalism of generalised standard materials, initially developed for hard condensed matter, will probably require specific modelling efforts to incorporate features of soft condensed matter and biophysics, such as progressive onset of plasticity due to cell contour fluctuations, two-phase coexistence corresponding to multiple minima in the energy or dissipation functions, or deformation-dependent terms in the dissipation function.

Facing this task, it is important to determine the best approach in representing and correlating various fields, in order to obtain a more intuitive grasp of the relative importance of various couplings. Quite generally, genetic engineering or pharmacological treatment can help discriminate the contribution made by a particular ingredient. For instance, computing the differences between wild-type tissues and mutants enables to delineate separately the contribution of a single ingredient within a complex feedback network, and to further validate a model.

In the more distant perspective of integrating ingredients from genetics with mechanical models to fully understand morphogenetic processes, some questions should be considered. What kind of model parameters can be extracted from state-of-the-art experimental data? What minimal set of data is required to extract the parameters associated with a given class of models? Or reciprocally, given a modelling framework, what set of minimal experiments are necessary for validation and parameter extraction? Can we discriminate among models on the basis of their capacity to interpret the data in the most economical way?

It is a pleasure to thank Isabelle Bonnet, Ibrahim Cheddadi, H el ene Delano e-Ayari, Guillaume Gr egoire, Shuji Ishihara, Pierre Recho, Jean-Fran ois Rupprecht for a critical reading of the manuscript.

Appendix A. From discrete cells to tissue scale

Tools are required to link the scale of discrete cells with the global scale of the tissue treated as a continuous material. Appendix A.1 presents tensorial tools to describe cellular materials. Appendix A.2 focuses on the particular question of size and growth. Appendix A.3 incorporates growth in the dynamics, treated as a scalar for simplicity.

Appendix A.1. Tensorial tools to describe cellular materials

This appendix presents some descriptive tensors. They can be measured visually without any knowledge of either the physics or the biology that determine the tissue behaviour, nor of the past history of the tissue. These tensors are called static (respectively, kinematic) when they can be determined from still images (respectively, movies).

Blanchard *et al.* [111,112] measure separately the deformation rate and the cell shape changes. Their difference is attributed only to the net effect of cell rearrangements, which is thus indirectly estimated.

These measurements can be unified using the texture tensor, which enables a direct and independent measurement of the deformation rate, the cell shape changes and the rate of rearrangements [68]. Briefly, consider two cells which share an edge (fig. 16). In the 2D case, their centers of mass have coordinates $\mathbf{r}_1 = (x_1, y_1)$ and $\mathbf{r}_2 = (x_2, y_2)$. A pair of such cells is called a ‘‘link’’, characterised by the vector $\boldsymbol{\ell} = \mathbf{r}_2 - \mathbf{r}_1$ with coordinates $(X, Y) = (x_2 - x_1, y_2 - y_1)$. The link vector carries the information on link length and angle. The link matrix \mathbf{m} is defined as:

$$\mathbf{m} = \boldsymbol{\ell} \otimes \boldsymbol{\ell} = \boldsymbol{\ell} \boldsymbol{\ell}^T = \begin{pmatrix} X^2 & XY \\ YX & Y^2 \end{pmatrix}. \quad (\text{A.1})$$

It retains the information of link size and angle, but not of its sign. This measurement becomes multi-scale upon coarse-graining over some spatial domain, by performing averages over several links (fig. 16c); time averages over several images can be performed too. Averaging \mathbf{m} over a group of cells, at any chosen length and/or time scale, reduces the whole cell pattern to the information of deformation and anisotropy over the corresponding set of links, called its texture, $M = \langle \mathbf{m} \rangle$:

$$M = \langle \boldsymbol{\ell} \otimes \boldsymbol{\ell} \rangle = \langle \boldsymbol{\ell} \boldsymbol{\ell}^T \rangle = \begin{pmatrix} \langle X^2 \rangle & \langle XY \rangle \\ \langle YX \rangle & \langle Y^2 \rangle \end{pmatrix}. \quad (\text{A.2})$$

There exist two orthogonal axes (eigenvectors) in which M would be diagonal, with strictly positive eigenvalues

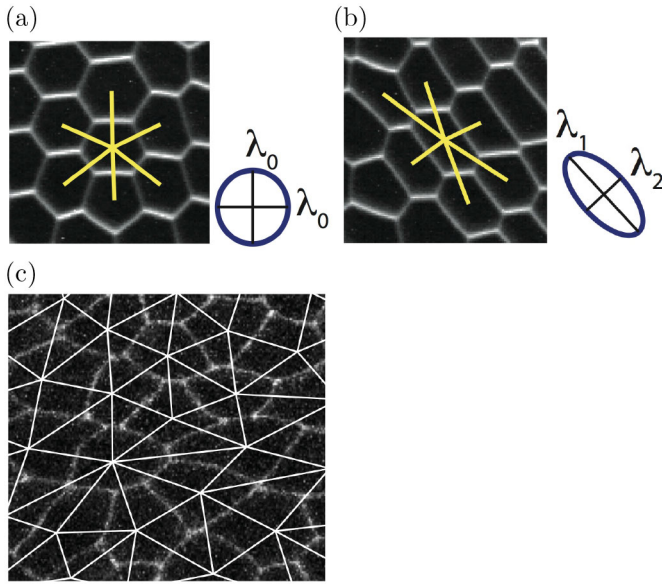


Fig. 16. Measurement of texture. (a) Snapshot of a foam, in an isotropic region; its texture has two equal eigenvalues. Straight lines, called “links”, are drawn between centers of neighbouring cells. (b) Same foam, in an anisotropic region; its texture has two different eigenvalues. (c) A tissue. Links are drawn over a whole region. Reprinted from [68].

λ_i ($i = 1$ or 2), of order of link mean square length in either direction. M is represented by an ellipse with axes proportional to the eigenvalues λ_i . It is more circular in fig. 16a than in fig. 16b.

Kinematic tensors such as the deformation rate, the cell shape changes and the rate of rearrangements can be expressed using the formalism based on this texture [68]. The cell shape changes correspond to the changes in texture. The links which appear (or disappear) in the time interval between two successive images of a movie characterise changes in the cell pattern topology and can be combined to measure the rearrangement rate contribution to the inter-cell deformation rate, $\dot{\epsilon}_{\text{inter}}$. All links which are conserved during the time interval between two successive images of a movie can be tracked: their changes express the relative motion of pairs of neighboring cells, and thus measure the velocity gradient, $\dot{\epsilon}$.

Appendix A.2. Volume

We show here that the average cell volume is related to the determinant of tensor M and use it to estimate the growth rate α_g from local measurements.

In 2D, let ℓ_1 , ℓ_2 and ℓ_3 be link vectors between three neighbouring cell centers. One can show that

$$\begin{aligned} & (\ell_1 \times \ell_2)^2 + (\ell_2 \times \ell_3)^2 + (\ell_3 \times \ell_1)^2 \\ &= \det(\ell_1 \otimes \ell_1 + \ell_2 \otimes \ell_2 + \ell_3 \otimes \ell_3). \end{aligned} \quad (\text{A.3})$$

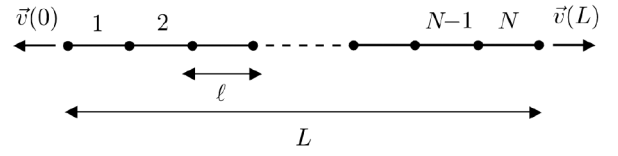


Fig. 17. Notations for the discrete approach of growth. A one-dimensional tissue of length L is made of N cells of length ℓ .

Hence, the surface area of the triangle, $S_{123} = \frac{1}{2}|\ell_1 \times \ell_2|$, can be expressed as

$$S_{123} = \frac{1}{2\sqrt{3}} \sqrt{\det(\ell_1 \otimes \ell_1 + \ell_2 \otimes \ell_2 + \ell_3 \otimes \ell_3)}. \quad (\text{A.4})$$

In a large two-dimensional assembly, the number of such triangles is equal to twice the number of cell centers [72]. Hence, the average surface area per cell is

$$\begin{aligned} \langle S_{\text{cell}} \rangle &\approx 2 \langle S_{123} \rangle \\ &= \frac{1}{\sqrt{3}} \langle \sqrt{\det(\ell_1 \otimes \ell_1 + \ell_2 \otimes \ell_2 + \ell_3 \otimes \ell_3)} \rangle \\ &\approx \sqrt{3} \sqrt{\det(M)}. \end{aligned} \quad (\text{A.5})$$

In 3D, a similar relation holds for the cell volume

$$\langle V_{\text{cell}} \rangle \propto \sqrt{\det(M)}. \quad (\text{A.6})$$

Hence, both in 2D and 3D, the growth rate α_g is approximately:

$$\alpha_g \approx \frac{1}{2} \frac{d(\det M)}{\det M} \frac{dt}{dt}. \quad (\text{A.7})$$

Note that eq. (A.7) becomes exact when M is replaced by the similar tensor B [69]. It relates vectors ℓ_0 located on a circle in the relaxed configuration with vectors ℓ on an ellipse in the current configuration ($\ell^T B^{-1} \ell = \ell_0^T \ell_0$), so that $B = I$ in a relaxed configuration, where I denotes the unit tensor.

Appendix A.3. Growth: discrete and continuous descriptions

In the present appendix, we derive and interpret eq. (32). We discuss how to start from a discrete description of the effect of growth in the tissue, to derive the corresponding continuum description, first in kinematics, then in dynamics. For simplicity, we treat here a one-dimensional tissue of length L , made of N cells of same length ℓ , mass m , spring constant K and rest length ℓ_0 (fig. 17):

$$L = N\ell. \quad (\text{A.8})$$

Appendix A.3.1. Kinematics

The tissue mass is $M = Nm$, and the growth rate α_g obeys

$$\frac{dN}{dt} = \alpha_g N. \quad (\text{A.9})$$

Meanwhile, the Eulerian elongation rate $\dot{\varepsilon}$ (eq. (11)) obeys

$$\frac{dL}{dt} = \dot{\varepsilon}L. \quad (\text{A.10})$$

Differentiating eq. (A.8) with respect to time and using eqs. (A.9), (A.10) yields the time evolution of the cell length ℓ

$$\frac{1}{\ell} \frac{d\ell}{dt} = \dot{\varepsilon} - \alpha_g. \quad (\text{A.11})$$

The cell elongation rate is thus the difference between the tissue elongation rate and the growth rate.

Appendix A.3.2. Dynamics

Within the limit of small elastic deformations, the cell elongation $\ell - \ell_0$ determines the stress σ and the elastically stored part of the deformation

$$\sigma = K(\ell - \ell_0), \quad (\text{A.12})$$

$$\varepsilon_e = \frac{\ell - \ell_0}{\ell_0}. \quad (\text{A.13})$$

Combining eq. (A.11) with eq. (A.13) yields

$$\dot{\varepsilon}_e = (\dot{\varepsilon} - \alpha_g) \frac{\ell}{\ell_0} = (1 + \varepsilon_e)(\dot{\varepsilon} - \alpha_g) \quad (\text{A.14})$$

so that, still in the limit of small deformations

$$\dot{\varepsilon}_e \simeq \dot{\varepsilon} - \alpha_g. \quad (\text{A.15})$$

Injecting eqs. (A.12), (A.13) into the continuum elasticity eq. (34) yields the elastic modulus of a tissue

$$G \equiv K \ell_0 \quad (\text{A.16})$$

which, combined with eq. (A.15), yields the stress evolution eq. (32).

At large deformations (see appendix D), eq. (A.13) admits several possible generalisations, see for instance eq. (D.17), each of which in turn yields a slightly different version of eq. (A.15), and thus of eq. (32).

Appendix B. Rheological diagrams and dissipation function

Within the dissipation function formalism, appendix B.1 explains how to derive equations when starting from a rheological diagram. Appendix B.2 explicits calculations for tensors, while appendix B.3 examines their incompressible case. Appendix B.4 shows recursively that any rheological diagram can be included, whatever its complexity.

Appendix B.1. Deriving equations

This appendix retraces practical calculations on a simple example. It shows that the formalism of eqs. (3)-(6) with $m = 1$ can describe the diagram discussed in sect. 2.2.1, yielding eq. (2).

When conducting explicitly the calculations outlined in sect. 2.2.3, there are redundant variables. They can be eliminated by taking into account the topological relations of the diagram. For instance, the diagram represented in fig. 1 involves three different deformation rates which are not independent: $\dot{\varepsilon}$, $\dot{\varepsilon}_1$ and $\dot{\varepsilon}_2$. A naive formulation of the energy and dissipation functions would read

$$\mathcal{E} = \frac{1}{2} G_1 \varepsilon_1^2, \quad (\text{B.1})$$

$$\mathcal{D} = \frac{1}{2} \eta_1 \dot{\varepsilon}_2^2 + \frac{1}{2} \eta_2 \dot{\varepsilon}^2. \quad (\text{B.2})$$

The topology of the diagram provides the relationship between the deformation variables

$$\varepsilon = \varepsilon_1 + \varepsilon_2, \quad (\text{B.3})$$

$$\dot{\varepsilon} = \dot{\varepsilon}_1 + \dot{\varepsilon}_2. \quad (\text{B.4})$$

Note that in the dissipation function formalism, internal variables must be independent. Each spring should be associated with one of the chosen, independent variables, such as ε_1 . Equations (B.3), (B.4) enable to drop one of the internal variables, for instance ε_2

$$\mathcal{E}(\varepsilon, \varepsilon_1) = \frac{1}{2} G_1 \varepsilon_1^2, \quad (\text{B.5})$$

$$\mathcal{D}(\dot{\varepsilon}, \dot{\varepsilon}_1) = \frac{1}{2} \eta_1 (\dot{\varepsilon} - \dot{\varepsilon}_1)^2 + \frac{1}{2} \eta_2 \dot{\varepsilon}^2. \quad (\text{B.6})$$

Equations (5), (6) with $m = 1$ yield

$$\sigma = \eta_1 (\dot{\varepsilon} - \dot{\varepsilon}_1) + \eta_2 \dot{\varepsilon}, \quad (\text{B.7})$$

$$0 = G_1 \varepsilon_1 + \eta_1 (\dot{\varepsilon}_1 - \dot{\varepsilon}). \quad (\text{B.8})$$

Eliminating ε_1 and $\dot{\varepsilon}_1$ between eqs. (B.7), (B.8) indeed yields eq. (2).

Appendix B.2. Tensorial case and example

This appendix generalizes the explicit calculations of sect. B.1 to a tensorial case and provides an example. The large deformation case is treated in appendices D.2.3 and D.2.4.

It is convenient to decompose each deformation tensor, such as ε , into two independent parts: an isotropic part which alters the volume and is proportional to the trace $\text{tr} \varepsilon$ of the tensor, and an anisotropic part which affects the shape and is the tensor deviator $\text{dev} \varepsilon = \varepsilon - \frac{1}{d} \text{tr} \varepsilon I$

$$\varepsilon = \frac{1}{d} \text{tr} \varepsilon I + \text{dev} \varepsilon, \quad (\text{B.9})$$

where I denotes the unit tensor.

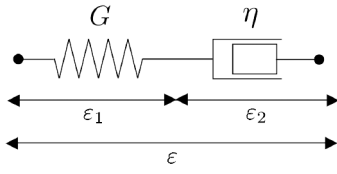


Fig. 18. A Maxwell viscoelastic liquid.

Since the deformation ε is now split into two independent variables $\text{tr } \varepsilon$ and $\text{dev } \varepsilon$, the expression of the stress (eq. (5)) must be reconsidered. Since \mathcal{E} and \mathcal{D} are scalars, the expression derived through differentiation with respect to $\text{dev } \dot{\varepsilon}$ and $\text{dev } \varepsilon$ is also a traceless tensor. It is thus naturally identified with $\text{dev } \sigma$

$$\text{dev } \sigma = \frac{\partial \mathcal{D}}{\partial \text{dev } \dot{\varepsilon}} + \frac{\partial \mathcal{E}}{\partial \text{dev } \varepsilon}. \quad (\text{B.10})$$

Finally, the corresponding expression with traces is a scalar and is identified with $\text{tr } \sigma$

$$\text{tr } \sigma = \frac{\partial \mathcal{D}}{\partial \text{tr } \dot{\varepsilon}} + \frac{\partial \mathcal{E}}{\partial \text{tr } \varepsilon}. \quad (\text{B.11})$$

The same decomposition, applied to eq. (6), yields

$$0 = \frac{\partial \mathcal{D}}{\partial \text{dev } \dot{\varepsilon}_k} + \frac{\partial \mathcal{E}}{\partial \text{dev } \varepsilon_k}, \quad (\text{B.12})$$

$$0 = \frac{\partial \mathcal{D}}{\partial \text{tr } \dot{\varepsilon}_k} + \frac{\partial \mathcal{E}}{\partial \text{tr } \varepsilon_k}. \quad (\text{B.13})$$

As an example, we choose for simplicity to treat a Maxwell viscoelastic liquid (fig. 18, equivalent to fig. 1 with $\eta_2 = 0$). In the compressible case, the stress is the sum of the following elastic and viscous contributions delimited by square brackets:

$$\sigma = [2G \text{dev } \varepsilon_1 + K \text{tr } \varepsilon_1 I] + [2\eta (\text{dev } \dot{\varepsilon} - \text{dev } \dot{\varepsilon}_1) + \chi (\text{tr } \dot{\varepsilon} - \text{tr } \dot{\varepsilon}_1) I]. \quad (\text{B.14})$$

The constitutive equation (B.14) can be decomposed into trace and deviator, which in the present example yields

$$\text{tr } \sigma = \chi d (\text{tr } \dot{\varepsilon} - \text{tr } \dot{\varepsilon}_1), \quad (\text{B.15})$$

$$\text{dev } \sigma = 2\eta (\text{dev } \dot{\varepsilon} - \text{dev } \dot{\varepsilon}_1), \quad (\text{B.16})$$

$$0 = K d \text{tr } \varepsilon_1 + \chi d (\text{tr } \dot{\varepsilon}_1 - \text{tr } \dot{\varepsilon}), \quad (\text{B.17})$$

$$0 = 2G \text{dev } \varepsilon_1 + 2\eta (\text{dev } \dot{\varepsilon}_1 - \text{dev } \dot{\varepsilon}). \quad (\text{B.18})$$

Coming back to energy and dissipation functions, trace and deviatoric components can be considered as independent variables

$$\mathcal{E} = G (\text{dev } \varepsilon_1)^2 + \frac{1}{2} K (\text{tr } \varepsilon_1)^2, \quad (\text{B.19})$$

$$\mathcal{D} = \eta (\text{dev } \dot{\varepsilon} - \text{dev } \dot{\varepsilon}_1)^2 + \frac{1}{2} \chi (\text{tr } \dot{\varepsilon} - \text{tr } \dot{\varepsilon}_1)^2. \quad (\text{B.20})$$

Using eqs. (B.10)-(B.13) with eqs. (B.19)-(B.20) yields eqs. (B.15)-(B.18), as expected.

Appendix B.3. Incompressible case

The incompressible limit occurs when the parameters K and χ go to infinity while the stress remains finite. The degrees of freedom for volume change represented by the trace of the deformations and deformation rates are frozen. They should therefore be absent from the energy and dissipation expressions, and $\text{tr } \sigma$ is undetermined.

In the case of a Maxwell viscoelastic liquid (fig. 18), eqs. (B.19), (B.20) for the energy and dissipation functions become

$$\mathcal{E} = G (\text{dev } \varepsilon_1)^2, \quad (\text{B.21})$$

$$\mathcal{D} = \eta (\text{dev } \dot{\varepsilon} - \text{dev } \dot{\varepsilon}_1)^2. \quad (\text{B.22})$$

Using eqs. (B.10)-(B.13), the resulting equations are identical to eqs. (B.16), (B.18):

$$\text{dev } \sigma = 2\eta (\text{dev } \dot{\varepsilon} - \text{dev } \dot{\varepsilon}_1), \quad (\text{B.23})$$

$$0 = 2G \text{dev } \varepsilon_1 + 2\eta (\text{dev } \dot{\varepsilon}_1 - \text{dev } \dot{\varepsilon}). \quad (\text{B.24})$$

Appendix B.4. Recursive construction of dissipation function

We show here that *any rheological diagram* can be described within the dissipation function formalism. The basic ingredients (*e.g.* a dashpot, a slider, a viscoelastic element, etc.) have been studied in the main text, particularly in sect. 3, and successfully described within the dissipation function formalism. An arbitrarily complex rheological diagram can be generated by successive combinations, either in parallel or in series, of simpler subdiagrams. We need to prove recursively that constitutive equations obtained directly from an arbitrary rheological diagram are identical to those obtained from eqs. (5), (6) within the dissipation function formalism.

Let \mathcal{S}_α be a first subdiagram with total deformation ε_α , total deformation rate $\dot{\varepsilon}_\alpha$, m_α internal variables ε_k ($1 \leq k \leq m_\alpha$), a free energy $\mathcal{E}_\alpha(\varepsilon_\alpha, \varepsilon_1, \dots, \varepsilon_{m_\alpha})$ and a dissipation function $\mathcal{D}_\alpha(\dot{\varepsilon}_\alpha, \dot{\varepsilon}_1, \dots, \dot{\varepsilon}_{m_\alpha})$. Then eqs. (3), (4) write

$$\sigma_\alpha = \frac{\partial \mathcal{D}_\alpha}{\partial \dot{\varepsilon}_\alpha} + \frac{\partial \mathcal{E}_\alpha}{\partial \varepsilon_\alpha}, \quad (\text{B.25})$$

$$0 = \frac{\partial \mathcal{D}_\alpha}{\partial \dot{\varepsilon}_k} + \frac{\partial \mathcal{E}_\alpha}{\partial \varepsilon_k}, \quad 1 \leq k \leq m_\alpha, \quad (\text{B.26})$$

where σ_α denotes the stress of subdiagram \mathcal{S}_α . Similarly, a second subdiagram \mathcal{S}_β is defined with m_β internal variables, and constitutive equations given by

$$\sigma_\beta = \frac{\partial \mathcal{D}_\beta}{\partial \dot{\varepsilon}_\beta} + \frac{\partial \mathcal{E}_\beta}{\partial \varepsilon_\beta}, \quad (\text{B.27})$$

$$0 = \frac{\partial \mathcal{D}_\beta}{\partial \dot{\varepsilon}_k} + \frac{\partial \mathcal{E}_\beta}{\partial \varepsilon_k}, \quad m_\alpha + 1 \leq k \leq m_\alpha + m_\beta. \quad (\text{B.28})$$

The total free energy and dissipation functions of the combined diagram $\mathcal{S} = \mathcal{S}_\alpha \cup \mathcal{S}_\beta$ are formally defined as

$$\mathcal{E} = \mathcal{E}_\alpha + \mathcal{E}_\beta, \quad (\text{B.29})$$

$$\mathcal{D} = \mathcal{D}_\alpha + \mathcal{D}_\beta. \quad (\text{B.30})$$

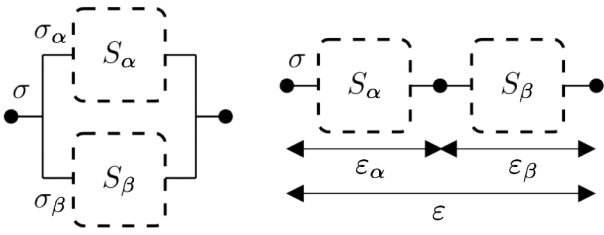


Fig. 19. Two subdiagrams S_α and S_β in parallel (left) and in series (right) with their respective deformations ε_α , ε_β and stresses σ_α , σ_β .

The next sections show that when S_α and S_β are combined either in parallel (sect. B.4.1) or in series (sect. B.4.2), a proper choice of independent variables for \mathcal{E} and \mathcal{D} yields the expected constitutive equations for \mathcal{S}

$$\sigma = \frac{\partial \mathcal{D}}{\partial \dot{\varepsilon}} + \frac{\partial \mathcal{E}}{\partial \varepsilon}, \quad (\text{B.31})$$

$$0 = \frac{\partial \mathcal{D}}{\partial \dot{\varepsilon}_k} + \frac{\partial \mathcal{E}}{\partial \varepsilon_k}, \quad (\text{B.32})$$

in agreement with the mechanical equations relating σ to σ_α , σ_β , and ε to ε_α , ε_β (fig. 19).

Appendix B.4.1. Two subdiagrams in parallel

We consider here the combination in parallel of S_α and S_β , with identical deformation and deformation rate (see fig. 19, left)

$$\varepsilon = \varepsilon_\alpha = \varepsilon_\beta, \quad (\text{B.33})$$

$$\dot{\varepsilon} = \dot{\varepsilon}_\alpha = \dot{\varepsilon}_\beta. \quad (\text{B.34})$$

Here, S_α and S_β can be decoupled or coupled.

We first examine the case where S_α and S_β are decoupled (no duplicate internal variables). This is the case for subdiagrams composed of mechanical elements only: all internal variables pertaining to S_α are distinct from all internal variables pertaining to S_β . The energy and dissipation functions depend on the following independent variables:

$$\mathcal{E} = \mathcal{E}(\varepsilon, \varepsilon_1, \dots, \varepsilon_{m_\alpha+m_\beta}), \quad (\text{B.35})$$

$$\mathcal{D} = \mathcal{D}(\dot{\varepsilon}, \dot{\varepsilon}_1, \dots, \dot{\varepsilon}_{m_\alpha+m_\beta}). \quad (\text{B.36})$$

Equations (B.26), (B.28) yield eq. (B.32) for all internal variables of \mathcal{S} , $1 \leq k \leq m_\alpha + m_\beta$. The expression for the stress σ of the combined diagram \mathcal{S} is correct

$$\begin{aligned} \sigma &= \frac{\partial \mathcal{D}}{\partial \dot{\varepsilon}} + \frac{\partial \mathcal{E}}{\partial \varepsilon} \\ &= \left(\frac{\partial \mathcal{D}_\alpha}{\partial \dot{\varepsilon}} + \frac{\partial \mathcal{D}_\beta}{\partial \dot{\varepsilon}} \right) + \left(\frac{\partial \mathcal{E}_\alpha}{\partial \varepsilon} + \frac{\partial \mathcal{E}_\beta}{\partial \varepsilon} \right) \\ &= \left(\frac{\partial \mathcal{D}_\alpha}{\partial \dot{\varepsilon}_\alpha} + \frac{\partial \mathcal{D}_\beta}{\partial \dot{\varepsilon}_\beta} \right) + \left(\frac{\partial \mathcal{E}_\alpha}{\partial \varepsilon_\alpha} + \frac{\partial \mathcal{E}_\beta}{\partial \varepsilon_\beta} \right) \\ &= \sigma_\alpha + \sigma_\beta. \end{aligned} \quad (\text{B.37})$$

Second, we examine the case where S_α and S_β are coupled. This is the case if non-mechanical internal variables couple to mechanical internal variables of both S_α and S_β . Duplicates must then be eliminated when selecting independent internal variables of \mathcal{S} . For convenience, we order internal variables as:

$$\mathcal{E}_\alpha(\varepsilon_\alpha, \varepsilon_1, \dots, \varepsilon_p, \varepsilon_{p+1}, \dots, \varepsilon_{m_\alpha}),$$

$$\mathcal{E}_\beta(\varepsilon_\beta, \varepsilon_{m_\alpha+1}, \dots, \varepsilon_{m_\beta+p}, \varepsilon_{m_\beta+p+1}, \dots, \varepsilon_{m_\alpha+m_\beta}),$$

with $m_\alpha - (p+1)$ duplicate variables $\varepsilon_k = \varepsilon_{m_\beta+k}$, $p+1 \leq k \leq m_\alpha$. Pruning redundant variables yields the following choice of independent variables for \mathcal{S}

$$\mathcal{E}(\varepsilon, \varepsilon_1, \dots, \varepsilon_p, \varepsilon_{p+1}, \dots, \varepsilon_{m_\alpha}, \varepsilon_{m_\alpha+1}, \dots, \varepsilon_{m_\beta+p}),$$

$$\mathcal{D}(\dot{\varepsilon}, \dot{\varepsilon}_1, \dots, \dot{\varepsilon}_p, \dot{\varepsilon}_{p+1}, \dots, \dot{\varepsilon}_{m_\alpha}, \dot{\varepsilon}_{m_\alpha+1}, \dots, \dot{\varepsilon}_{m_\beta+p})$$

(compare with eqs. (B.35), (B.36)), while eq. (B.37) is unchanged, and we check that, for the initially redundant variables, *i.e.*, for $p+1 \leq k \leq m_\alpha$

$$\begin{aligned} \frac{\partial \mathcal{D}}{\partial \dot{\varepsilon}_k} + \frac{\partial \mathcal{E}}{\partial \varepsilon_k} &= \left(\frac{\partial \mathcal{D}_\alpha}{\partial \dot{\varepsilon}_k} + \frac{\partial \mathcal{E}_\alpha}{\partial \varepsilon_k} \right) + \left(\frac{\partial \mathcal{D}_\beta}{\partial \dot{\varepsilon}_{m_\beta+k}} + \frac{\partial \mathcal{E}_\beta}{\partial \varepsilon_{m_\beta+k}} \right) \\ &= 0 + 0 \\ &= 0. \end{aligned} \quad (\text{B.38})$$

Appendix B.4.2. Two subdiagrams in series

We consider here the combination in series of S_α and S_β (see fig. 19, right). Since

$$\varepsilon = \varepsilon_\alpha + \varepsilon_\beta, \quad (\text{B.39})$$

$$\dot{\varepsilon} = \dot{\varepsilon}_\alpha + \dot{\varepsilon}_\beta, \quad (\text{B.40})$$

we (arbitrarily) choose to keep ε_α and $\dot{\varepsilon}_\alpha$ rather than ε_β and $\dot{\varepsilon}_\beta$ as independent variables.

In the absence of duplicate internal variables between S_α and S_β , we choose as independent variables

$$\mathcal{E}(\varepsilon, \varepsilon_1, \dots, \varepsilon_{m_\alpha+m_\beta}, \varepsilon_\alpha),$$

$$\mathcal{D}(\dot{\varepsilon}, \dot{\varepsilon}_1, \dots, \dot{\varepsilon}_{m_\alpha+m_\beta}, \dot{\varepsilon}_\alpha).$$

For $1 \leq k \leq m_\alpha$ (respectively, $m_\alpha + 1 \leq k \leq m_\beta$), eq. (B.32) is identical to eq. (B.26) (respectively, eq. (B.28)).

We next consider the change of variables $(\varepsilon_\alpha, \varepsilon_\beta) \rightarrow (\varepsilon, \varepsilon_\alpha)$, $(\dot{\varepsilon}_\alpha, \dot{\varepsilon}_\beta) \rightarrow (\dot{\varepsilon}, \dot{\varepsilon}_\alpha)$. Since

$$\frac{\partial}{\partial \varepsilon |_{\varepsilon_\alpha}} = \frac{\partial}{\partial \varepsilon_\beta |_{\varepsilon_\alpha}},$$

$$\frac{\partial}{\partial \varepsilon_\alpha |_{\varepsilon}} = \frac{\partial}{\partial \varepsilon_\alpha |_{\varepsilon_\beta}} - \frac{\partial}{\partial \varepsilon_\beta |_{\varepsilon_\alpha}}$$

(and similar expressions involving the rates of deformation) we deduce

$$\frac{\partial \mathcal{E}}{\partial \varepsilon |_{\varepsilon_\alpha}} = \frac{\partial \mathcal{E}_\beta}{\partial \varepsilon_\beta |_{\varepsilon_\alpha}},$$

$$\frac{\partial \mathcal{D}}{\partial \dot{\varepsilon} |_{\dot{\varepsilon}_\alpha}} = \frac{\partial \mathcal{D}_\beta}{\partial \dot{\varepsilon}_\beta |_{\dot{\varepsilon}_\alpha}}$$

and

$$\sigma = \sigma_\beta,$$

using eqs. (B.27), (B.31). Further, since

$$\begin{aligned} \frac{\partial \mathcal{E}}{\partial \varepsilon_\alpha | \varepsilon} &= \frac{\partial \mathcal{E}_\alpha}{\partial \varepsilon_\alpha | \varepsilon_\beta} - \frac{\partial \mathcal{E}_\beta}{\partial \varepsilon_\beta | \varepsilon_\alpha}, \\ \frac{\partial \mathcal{D}}{\partial \dot{\varepsilon}_\alpha | \dot{\varepsilon}} &= \frac{\partial \mathcal{D}_\alpha}{\partial \dot{\varepsilon}_\alpha | \dot{\varepsilon}_\beta} - \frac{\partial \mathcal{D}_\beta}{\partial \dot{\varepsilon}_\beta | \dot{\varepsilon}_\alpha}, \end{aligned}$$

we also have

$$\begin{aligned} \sigma_\alpha - \sigma_\beta &= \left(\frac{\partial \mathcal{D}_\alpha}{\partial \dot{\varepsilon}_\alpha} + \frac{\partial \mathcal{E}_\alpha}{\partial \varepsilon_\alpha} \right) - \left(\frac{\partial \mathcal{D}_\beta}{\partial \dot{\varepsilon}_\beta} + \frac{\partial \mathcal{E}_\beta}{\partial \varepsilon_\beta} \right) \\ &= \frac{\partial \mathcal{D}}{\partial \dot{\varepsilon}_\alpha | \dot{\varepsilon}} + \frac{\partial \mathcal{E}}{\partial \varepsilon_\alpha | \varepsilon} \\ &= 0, \end{aligned} \quad (\text{B.41})$$

so that $\sigma_\alpha = \sigma_\beta$, in agreement with the rheological diagram (fig. 19, right).

If there are duplicate internal variables, they can be treated as in sect. B.4.1, with the choice

$$\begin{aligned} \mathcal{E}(\varepsilon, \varepsilon_1, \dots, \varepsilon_{m_\alpha}, \varepsilon_{m_\alpha+1}, \dots, \varepsilon_{m_\beta+p}, \varepsilon_\alpha), \\ \mathcal{D}(\dot{\varepsilon}, \dot{\varepsilon}_1, \dots, \dot{\varepsilon}_{m_\alpha}, \dot{\varepsilon}_{m_\alpha+1}, \dots, \dot{\varepsilon}_{m_\beta+p}, \dot{\varepsilon}_\alpha). \end{aligned}$$

Appendix C. Scalar or polar non-mechanical field

Section 3.4 introduces the coupling of a tensorial non-mechanical field to a rheological model. This appendix presents the case of a scalar (appendix C.1) or polar (appendix C.2) field.

Appendix C.1. Scalar field

A usual example of a scalar field is the concentration field c of a morphogen [15] or of a relevant signaling molecule (see [113] for a more complex case). The energy \mathcal{E} and the dissipation function \mathcal{D} depend on the fields $(\varepsilon, \varepsilon_k, c)$ and $(\dot{\varepsilon}, \dot{\varepsilon}_k, \dot{c})$, respectively. This and other similar choices made below would need to be carefully validated by comparison with experimental data in specific cases.

Let us treat an example which couples the scalar field to the mechanical fields through the dissipation function. In one spatial dimension, we consider the case of a Maxwell viscoelastic liquid (fig. 18). Its usual evolution equation is $\dot{\sigma} + \sigma/\tau = G\dot{\varepsilon}$, where $\tau = \eta/G$ is the viscoelastic time. It is modified in the presence of a coupled field, for instance a morphogen concentration c .

We choose for instance to couple ε_2 and c through their time derivatives, and select ε and ε_2 as independent variables together with c . Equations (3), (4) become, with $m = 2$ internal variables:

$$\mathcal{E}(\varepsilon, \varepsilon_2, c) = \frac{1}{2}G(\varepsilon - \varepsilon_2)^2 + \frac{1}{2}\chi c^2, \quad (\text{C.1})$$

$$\mathcal{D}(\dot{\varepsilon}, \dot{\varepsilon}_2, \dot{c}) = \frac{1}{2}\eta\dot{\varepsilon}_2^2 + \frac{1}{2}\xi\dot{c}^2 + \beta\dot{\varepsilon}_2\dot{c}. \quad (\text{C.2})$$

To ensure the convexity of the dissipation function, the parameters G , χ , η and ξ are non-negative, β is a dissipative coupling coefficient which obeys

$$\beta^2 \leq \xi\eta. \quad (\text{C.3})$$

Equations (5), (6) yield the expression of the stress

$$\sigma = \frac{\partial \mathcal{D}}{\partial \dot{\varepsilon}} + \frac{\partial \mathcal{E}}{\partial \varepsilon} = G(\varepsilon - \varepsilon_2) \quad (\text{C.4})$$

and two evolution equations

$$0 = \frac{\partial \mathcal{D}}{\partial \dot{\varepsilon}_2} + \frac{\partial \mathcal{E}}{\partial \varepsilon_2} = \eta\dot{\varepsilon}_2 - G(\varepsilon - \varepsilon_2) + \beta\dot{c}, \quad (\text{C.5})$$

$$0 = \frac{\partial \mathcal{D}}{\partial \dot{c}} + \frac{\partial \mathcal{E}}{\partial c} = \xi\dot{c} + \chi c + \beta\dot{\varepsilon}_2. \quad (\text{C.6})$$

Injecting eq. (C.4) and its time derivative into eq. (C.5), we find the evolution equation for the stress field

$$\dot{\sigma} + \frac{\sigma}{\tau} = G\dot{\varepsilon} + \frac{\beta}{\tau}\dot{c}. \quad (\text{C.7})$$

Similarly, eliminating $\dot{\varepsilon}_2$ between eqs. (C.5), (C.6), then injecting eq. (C.4), yields the evolution equation for the scalar field c

$$\dot{c} + \frac{c}{\tau_c} = -\frac{\beta}{\eta\xi - \beta^2}\sigma, \quad (\text{C.8})$$

with a relaxation time for the concentration

$$\tau_c = \frac{\xi\eta - \beta^2}{\chi\eta}.$$

Here τ_c is positive due to eq. (C.3) and its inverse τ_c^{-1} is for instance the degradation rate of the morphogen. Using eq. (C.8), we eliminate \dot{c} in eq. (C.7) and find

$$\dot{\sigma} + \frac{\sigma}{\tau_\sigma} = G\dot{\varepsilon} - \frac{G\beta\chi}{\eta\xi - \beta^2}c, \quad (\text{C.9})$$

where the stress relaxation time

$$\tau_\sigma = \frac{\xi\eta - \beta^2}{\xi G}$$

is shorter than the usual viscoelastic time $\tau = \eta/G$ as soon as the coupling β is non-zero.

In the long time limit, the rheology is viscous: all relevant fields are proportional to each other, at least in this linear regime. The effective viscosity $\eta_{\text{eff}} = G\tau_\sigma$ is smaller than η as soon as the coupling β is non-zero; $\sigma/\dot{\varepsilon}$ and $c/\dot{\varepsilon}$ tend towards constants (compare with eqs. (54)-(57))

$$\frac{\sigma}{\dot{\varepsilon}} \rightarrow \eta_{\text{eff}} = \eta - \frac{\beta^2}{\xi}, \quad (\text{C.10})$$

$$\frac{c}{\dot{\varepsilon}} \rightarrow \frac{\beta}{\chi} \frac{\eta_{\text{eff}}}{\eta} = \frac{\beta}{\xi} \left(1 - \frac{\beta^2}{\eta\xi} \right). \quad (\text{C.11})$$

Appendix C.2. Polar field

Let us turn to the case of a polar non-mechanical field. For instance, in collectively migrating cells, a cell acquires a front-rear asymmetry manifested both in its shape and in intra-cellular protein distributions. Such cell scale asymmetry defines a vector field, the polarity \mathbf{p} [65,66], where \mathbf{p} and $-\mathbf{p}$ characterize opposite configurations. This is an example of a polar order parameter. Another, possibly related, example of polar order parameter is the gradient of a chemical concentration c , for instance a morphogen. Constitutive equations which include active couplings between polar and mechanical fields have also been proposed in [114].

When cells are elongated and rapidly switch front and back, a nematic order parameter may also be relevant to describe the collective migration of a cell monolayer [115]; such an axial order parameter is a particular case of a tensor and is considered in sect. 3.4.

We treat here for simplicity a case with one dimension of space, where \mathbf{e}_x is a unit vector, the polarity is $\mathbf{p} = p(x, t) \mathbf{e}_x$ and couples to a Maxwell viscoelastic liquid (fig. 18). When homogeneous polarity is preferred, the energy functional includes a term accounting for the cost of inhomogeneities of the polarity, with a prefactor (called ‘‘Frank constant’’) $K_F \geq 0$ [76]. The problem is invariant under the transformation $x \rightarrow -x$, $p \rightarrow -p$, allowing for instance for a coupling term between (elastic) deformation and polarity gradient in the energy function. The energy \mathcal{E} and the dissipation function \mathcal{D} depend on the fields $(\varepsilon, \varepsilon_1, p)$ and $(\dot{\varepsilon}, \dot{\varepsilon}_1, \dot{p})$, respectively. Assuming for simplicity no cross-coupling in the dissipation function, and eliminating ε_2 , eqs. (3), (4) read, with $m = 2$

$$\begin{aligned} \mathcal{E}(\varepsilon, \varepsilon_1, p) &= \frac{1}{2} G \varepsilon_1^2 + \frac{1}{2} \chi p^2 \\ &\quad + \frac{1}{2} K_F \left(\frac{\partial p}{\partial x} \right)^2 + \gamma \varepsilon_1 \frac{\partial p}{\partial x}, \end{aligned} \quad (\text{C.12})$$

$$\mathcal{D}(\dot{\varepsilon}, \dot{\varepsilon}_1, \dot{p}) = \frac{1}{2} \eta (\dot{\varepsilon} - \dot{\varepsilon}_1)^2 + \frac{1}{2} \xi \dot{p}^2, \quad (\text{C.13})$$

where G , χ , K_F , η and ξ are non-negative parameters, and $\gamma^2 \leq GK_F$ to ensure the convexity of \mathcal{E} . The stress

$$\sigma = \frac{\partial \mathcal{D}}{\partial \dot{\varepsilon}} + \frac{\partial \mathcal{E}}{\partial \varepsilon} = \eta (\dot{\varepsilon} - \dot{\varepsilon}_1) \quad (\text{C.14})$$

now depends on the polarity gradient through the additional relationship

$$0 = \frac{\partial \mathcal{D}}{\partial \dot{\varepsilon}_1} + \frac{\partial \mathcal{E}}{\partial \varepsilon_1} = -\eta (\dot{\varepsilon} - \dot{\varepsilon}_1) + G \varepsilon_1 + \gamma \frac{\partial p}{\partial x}. \quad (\text{C.15})$$

The evolution equation for the polar field is obtained after integration by parts

$$0 = \frac{\partial \mathcal{D}}{\partial \dot{p}} + \frac{\partial \mathcal{E}}{\partial p} = \xi \dot{p} + \chi p - K_F \frac{\partial^2 p}{\partial x^2} - \gamma \frac{\partial \varepsilon_1}{\partial x}. \quad (\text{C.16})$$

Combining eqs. (C.14), (C.16) we obtain a set of two coupled evolution equations for the stress and polarity field

$$\begin{aligned} \dot{\sigma} + \frac{G}{\eta} \sigma &= G \dot{\varepsilon} + \frac{\gamma^2}{G \xi} \frac{\partial^2 \sigma}{\partial x^2} - \frac{\gamma \chi}{\xi} \frac{\partial p}{\partial x} \\ &\quad + \gamma \frac{G K_F - \gamma^2}{G \xi} \frac{\partial^3 p}{\partial x^3}, \end{aligned} \quad (\text{C.17})$$

$$\dot{p} + \frac{\chi}{\xi} p = \frac{\gamma}{G \xi} \frac{\partial \sigma}{\partial x} + \frac{G K_F - \gamma^2}{G \xi} \frac{\partial^2 p}{\partial x^2}. \quad (\text{C.18})$$

The relaxation times for the polarity and stress are distinct.

Appendix D. Large elastic deformations of an incompressible and isotropic tissue

In the main text, the elastic deformations were considered small, even for large total tissue deformations. That is the condition for the linear formulation of the problem to be valid.

When the tissue undergoes large elastic deformations, the previous formalism must be modified in two ways. First, we derive a new expression for the evolution of the deformations, *i.e.* $\dot{\varepsilon}$ and all the $\dot{\varepsilon}_k$ s are replaced by the corresponding objective derivative; while this is standard in continuum mechanics, appendix D.1 precises its application to living tissues. Second, we formulate an adequate implementation of the dissipation function formalism, presented in appendix D.2.

In real tissues, the relaxed configuration of a given cell evolves both in shape and volume. For pedagogical reasons, we introduce simplifying assumptions:

- $\mathcal{H}1$: We assume that a relaxed local configuration has the same volume as the corresponding current configuration.
- $\mathcal{H}2$: We further assume that the relaxed local configuration is isotropic.

$\mathcal{H}1$ is reasonable since the short-time relaxation of a cell is likely to occur with conserved volume. $\mathcal{H}2$ simplifies the calculations. Both assumptions can be relaxed if needed, see [70].

Appendix D.1. Evolution of deformations

In the present appendix, we derive the time evolution equation of different deformations such as the total deformation ε (appendix D.1.1), its intra-cell contribution $\varepsilon_{\text{intra}}$ (appendix D.1.2) and its elastic part ε_e (appendix D.1.3). Appendix D.1.4 summarizes the resulting expressions.

Appendix D.1.1. Evolution without rearrangements

Here, we show that the objective derivative describing the evolution of a quantity attached to the material and which deforms with it, like the total deformation ε , is the upper-convected derivative.

We choose center-to-center vectors ℓ between neighbouring cells as described in appendix A.1. However, within a Lagrangian description, and in contrast with appendix A.1, let us now keep each end of each vector ℓ permanently attached to the very same cell. We construct a symmetric tensor

$$M_{\text{perm}} = \langle \ell \otimes \ell \rangle = \langle \ell \ell^T \rangle. \quad (\text{D.1})$$

When the material is subjected to a velocity field $\mathbf{v}(\mathbf{r})$, the tensor M_{perm} evolves as follows. After a time dt has elapsed, such a vector ℓ becomes

$$\ell' = (I + \xi)\ell, \quad (\text{D.2})$$

where we note $\xi \equiv \nabla \mathbf{v} dt$ with the convention $(\nabla \mathbf{v})_{ij} = \partial \mathbf{v}_i / \partial \mathbf{r}_j$. After averaging $\ell' \otimes \ell' - \ell \otimes \ell$ over vectors ℓ , eq. (D.2) yields

$$M'_{\text{perm}} - M_{\text{perm}} = \xi M_{\text{perm}} + M_{\text{perm}} \xi^T + \mathcal{O}(\xi^2). \quad (\text{D.3})$$

Dividing eq. (D.3) by dt and taking the limit $dt \rightarrow 0$ yields the time-derivative of M_{perm}

$$\left(\frac{\partial}{\partial t} + \mathbf{v} \cdot \nabla \right) M_{\text{perm}} = \nabla \mathbf{v} M_{\text{perm}} + M_{\text{perm}} \nabla \mathbf{v}^T. \quad (\text{D.4})$$

If M_{init} , the initial value of M_{perm} , is assumed isotropic (assumption $\mathcal{H}2$), we now define the deformation ε through:

$$M_{\text{perm}} = (I + 2\varepsilon) M_{\text{init}}. \quad (\text{D.5})$$

Injecting the definition of ε (eq. (D.5)) into eq. (D.4) yields its time evolution equation

$$\left(\frac{\partial}{\partial t} + \mathbf{v} \cdot \nabla \right) \varepsilon = D + \nabla \mathbf{v} \varepsilon + \varepsilon \nabla \mathbf{v}^T. \quad (\text{D.6})$$

The first term on the left-hand side of eq. (D.6) is the time derivative at a fixed point in space. Together with the second term, it constitutes the deformation rate $\dot{\varepsilon}$. This time derivative $\frac{\partial}{\partial t} + \mathbf{v} \cdot \nabla$ is the usual material derivative used also for scalar and vector quantities attached to a material with local velocity \mathbf{v} (eq. (10)). On the right-hand side, $D = (\nabla \mathbf{v} + \nabla \mathbf{v}^T)/2$ is the symmetric part of the velocity gradient. Conversely, the rotation rate $\Omega = (\nabla \mathbf{v} - \nabla \mathbf{v}^T)/2$ is the antisymmetric part of the velocity gradient. Equation (D.6) also reads

$$\dot{\varepsilon} = D + D\varepsilon + \varepsilon D + \Omega\varepsilon - \varepsilon\Omega. \quad (\text{D.7})$$

As long as the deformation is small, D is the main contribution to the evolution of the deformation. For simple viscous liquids, it is even often confused with the deformation rate. Similarly, for simple elastic solids, at small

deformation, the deformation is often defined as the symmetrised gradient of the displacement field, assimilating the symmetrised velocity gradient and the deformation rate. However, at large deformation, eq. (D.6) highlights the fact that the deformation rate $\dot{\varepsilon}$ and the symmetrised velocity gradient D are distinct, and this distinction is critical throughout the present appendix.

In fact, the last two terms on the right-hand side of eq. (D.6) are nonlinear, and become important at large deformation. They are specific to (rank two) tensors. They reflect the fact that the natural coordinates used to describe a tensor attached to the material are altered by the local velocity gradient. For instance, if the material is rotated as a solid, the tensor rotates in the same manner, or if the material is deformed, the coordinates are distorted. This implies that the time evolution of a tensor involves new terms that are of order 1 in the tensor [73,85,116,117].

Equation (D.6) can also be written as

$$\frac{\partial \varepsilon}{\partial t} + (\mathbf{v} \cdot \nabla) \varepsilon - \nabla \mathbf{v} \varepsilon - \varepsilon \nabla \mathbf{v}^T = D, \quad (\text{D.8})$$

where the left-hand side, also written $\overset{\nabla}{\varepsilon}$, is the so-called *upper-convective derivative* of ε . It is the only objective derivative that ensures that the dynamical equations respect the principle of covariance [118]. The derivation from eq. (D.1) to eq. (D.8) shows that this particular objective derivative appears univocally for a tensor constructed from vectors which ends are attached to the material and thus transported by the velocity field.

Appendix D.1.2. Evolution with rearrangements

To describe the evolution of the intra-cell contribution $\varepsilon_{\text{intra}}$ to the total deformation, it is useful to come back to the tensor M described in appendix A.1. It differs from the tensor M_{perm} discussed in sect. D.1.1 in one essential respect: the vectors ℓ are not attached permanently to cells. Instead, during each rearrangement, cells exchange neighbours, which redefines the list of vectors ℓ from which tensor M is constructed.

This effect on M must be incorporated into an evolution equation analogous to eq. (D.4)

$$\left(\frac{\partial}{\partial t} + \mathbf{v} \cdot \nabla \right) M = \nabla \mathbf{v} M + M \nabla \mathbf{v}^T - P. \quad (\text{D.9})$$

Here the rearrangement contribution P , introduced in [68], is a symmetric tensor defined as

$$P = \langle \ell_a \otimes \ell_a \delta(t - t_a) - \ell_d \otimes \ell_d \delta(t - t_d) \rangle \quad (\text{D.10})$$

where ℓ_a (respectively ℓ_d) are vectors which appear (resp. disappear) at times t_a (respectively t_d), and the average is taken over both space and time.

Since M is symmetric with strictly positive eigenvalues, its trace and determinant are non-zero, and it is in-

vertible. One can show that there exists a symmetric tensor D_p such that¹

$$P = D_p M + M D_p. \quad (\text{D.11})$$

Using eq. (D.11), eq. (D.9) can be re-written as

$$\left(\frac{\partial}{\partial t} + \mathbf{v} \cdot \nabla \right) M = W_{\text{intra}} M + M W_{\text{intra}}, \quad (\text{D.12})$$

where the *effective velocity gradient* is

$$W_{\text{intra}} = \nabla \mathbf{v} - D_p. \quad (\text{D.13})$$

If we define $\varepsilon_{\text{intra}}$ through

$$M = (I + 2\varepsilon_{\text{intra}}) M_{\text{init}}, \quad (\text{D.14})$$

then eq. (D.12) yields the time evolution equation of $\varepsilon_{\text{intra}}$

$$\begin{aligned} \left(\frac{\partial}{\partial t} + \mathbf{v} \cdot \nabla \right) \varepsilon_{\text{intra}} &= \frac{W_{\text{intra}} + W_{\text{intra}}^T}{2} \\ &+ W_{\text{intra}} \varepsilon_{\text{intra}} + \varepsilon_{\text{intra}} W_{\text{intra}}^T. \end{aligned} \quad (\text{D.15})$$

In other words, while the velocity gradient $\nabla \mathbf{v}$ acts onto the total tissue deformation ε (eq. (D.6)), the effective velocity gradient $W_{\text{intra}} = \nabla \mathbf{v} - D_p$ acts on the cell contribution to deformation $\varepsilon_{\text{intra}}$. Although W_{intra} and D_p have the dimension of an inverse time, like $\nabla \mathbf{v}$ or D , they do not derive from any actual vector field.

The rate of change of the intra-cell deformation $\varepsilon_{\text{intra}}$, expressed by eq. (D.15), can also be written in terms of the antisymmetric and symmetric parts of the effective velocity gradient W_{intra} , respectively Ω and $D_{\text{intra}} = D - D_p$

$$\begin{aligned} \dot{\varepsilon}_{\text{intra}} &= D_{\text{intra}} + \Omega \varepsilon_{\text{intra}} - \varepsilon_{\text{intra}} \Omega \\ &+ D_{\text{intra}} \varepsilon_{\text{intra}} + \varepsilon_{\text{intra}} D_{\text{intra}}. \end{aligned} \quad (\text{D.16})$$

¹ The demonstration goes as follows:

In one dimension, eq. (D.11) can be trivially inverted.

In two dimensions, using the Cayleigh-Hamilton theorem, $M^2 = (\text{tr } M)M + \frac{1}{2} \text{tr}(M^2)I - \frac{1}{2}(\text{tr } M)^2 I$, one can check that either of the following equivalent expressions satisfies eq. (D.11):

$$D_p = \frac{2P - MPM^{-1} - M^{-1}PM}{4} \text{tr } M + \frac{PM^{-1} - M^{-1}P}{4}$$

$$\text{or } D_p = \frac{\det M + (\text{tr } M)^2}{2 \text{tr } M \det M} P - \frac{MP + PM}{2 \det M} + \frac{MPM}{2 \text{tr } M \det M}.$$

In three dimensions, the Cayleigh-Hamilton theorem implies $M^3 = (\text{tr } M)M^2 + \frac{1}{2} \text{tr}(M^2)M - \frac{1}{2}(\text{tr } M)^2 M + (\det M)I$ and an expression that satisfies eq. (D.11) is

$$D_p = k_1 P + k_2 (MP + PM) + k_3 MPM + k_4 (M^2 P + P M^2) + k_5 (M^2 P M + M P M^2) + k_6 M^2 P M^2,$$

where:

$$k_1 = \frac{1}{r} [3 \det M (\text{tr } M)^2 + \text{tr}(M^3) \text{tr}(M^2) - \text{tr}(M^5)],$$

$$k_2 = \frac{1}{2r} [(\text{tr } M)^2 (\text{tr}(M^2) - (\text{tr } M)^2)],$$

$$k_3 = \frac{1}{r} [(\text{tr } M)^3 + \det M],$$

$$k_4 = 1/(2 \det M),$$

$$k_5 = -\frac{1}{r} (\text{tr } M)^2,$$

$$k_6 = \frac{1}{r} \text{tr } M,$$

$$r = [(\text{tr } M)^3 - \text{tr } M \text{tr}(M^2) - 2 \det M] \det M.$$

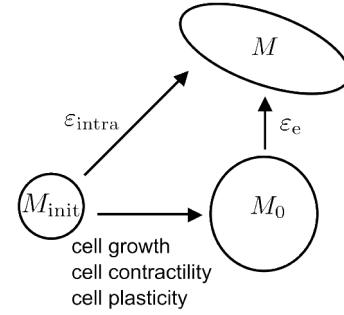


Fig. 20. Initial, current and rest local configuration of a piece of tissue are represented by symmetric tensors M_{init} , M and M_0 , respectively. The current and the rest configuration are related through the elastic deformation ε_e , the initial and current configuration are related through $\varepsilon_{\text{intra}}$, and the cell processes (growth, contractility, plasticity) modify the rest configuration. In appendix D.1.3, we do not consider cell contractility or cell plasticity, and we assume that M_0 is isotropic (assumption $\mathcal{H}2$).

Appendix D.1.3. Growth and elastic deformation

We now focus on the elastic part, pictured in fig. 20. If a piece of tissue in its current local configuration (represented by $M(t)$) was disconnected from its neighbourhood (for instance by circular laser ablation [26]), it would relax towards the relaxed configuration $M_0(t)$, which we assume isotropic (assumption $\mathcal{H}2$). We define the elastic deformation ε_e through

$$M(t) = (I + 2\varepsilon_e) M_0(t). \quad (\text{D.17})$$

In order to derive the evolution of ε_e , we now focus on the evolution of the relaxed state $M_0(t)$ as a result of intra-cell growth. For simplicity, we do not include here intra-cell plasticity and contractility. Assumption $\mathcal{H}2$ also excludes the combination of two successive deformations, which is beyond the scope of the present study, see [69, 93].

$M_0(t)$ is not necessarily accessible experimentally in a non-destructive manner. Yet under assumptions $\mathcal{H}1$ and $\mathcal{H}2$, $M_0(t)$ can be defined as the only isotropic tensor representing the same volume as $M(t)$. Taking into account eqs. (A.5), (A.6)

$$M_0(t) = (\det M(t))^{1/d} I = \left(\frac{\det M(t)}{\det M_{\text{init}}} \right)^{1/d} M_{\text{init}}. \quad (\text{D.18})$$

It follows from eqs. (A.7), (D.18) that

$$\frac{(\partial_t + \mathbf{v} \cdot \nabla) M_0}{M_0} \approx \frac{2}{d} \alpha_g I. \quad (\text{D.19})$$

Injecting eq. (D.17) into eq. (D.12), while using eq. (D.19) and the isotropy of M_0 , we obtain

$$\left(\frac{\partial}{\partial t} + \mathbf{v} \cdot \nabla \right) \varepsilon_e = \frac{W_e + W_e^T}{2} + W_e \varepsilon_e + \varepsilon_e W_e^T, \quad (\text{D.20})$$

where the effective velocity gradient is

$$W_e = \nabla \mathbf{v} - D_p - \alpha_g \frac{I}{d}. \quad (\text{D.21})$$

The effective velocity gradient W_e acts on the elastic deformation, ε_e . Equation (D.20) has the same structure as eq. (D.15).

The rate of change of the elastic deformation, ε_e , expressed by eq. (D.20), can also be written in terms of the antisymmetric and symmetric parts of the effective velocity gradient W_e , respectively $\Omega = (\nabla \mathbf{v} - \nabla \mathbf{v}^T)/2$ and $D_e = D - D_p - \alpha_g I/d$

$$\dot{\varepsilon}_e = D_e + \Omega \varepsilon_e - \varepsilon_e \Omega + D_e \varepsilon_e + \varepsilon_e D_e. \quad (\text{D.22})$$

Appendix D.1.4. Evolution of the (large) deformation: summary

Equations (D.7), (D.16), (D.22) read

$$\dot{\varepsilon} = (D + D\varepsilon + \varepsilon D) + (\Omega\varepsilon - \varepsilon\Omega), \quad (\text{D.23})$$

$$\dot{\varepsilon}_k = (D_k + D_k\varepsilon_k + \varepsilon_k D_k) + (\Omega\varepsilon_k - \varepsilon_k\Omega). \quad (\text{D.24})$$

Equations (D.23), (D.24) contain two parts delimited by parentheses. First, a part due to an effective symmetrised velocity gradient D_k which depends on k (and which is the true symmetrised velocity gradient D only in eq. (D.23)); second, another part due to the rotation rate Ω , which does not depend on k .

If Q_k is a non-mechanical tensor (sect. 3.4) constructed from a distribution of objects attached to element k of the rheological diagram, and if its rest value is isotropic, then its evolution is equal to its physical (intrinsic) rate of change $\dot{Q}_k^{\text{intrinsic}}$ corrected by transport terms, like in eq. (D.24)

$$\dot{Q}_k = (\dot{Q}_k^{\text{intrinsic}} + D_k Q_k + Q_k D_k) + (\Omega Q_k - Q_k \Omega). \quad (\text{D.25})$$

Appendix D.2. Dissipation function formalism at large deformation

The present appendix discusses how to implement large deformations within the dissipation function formalism. Appendix D.2.1 provides a possible expression for the elastic energy that is suitable for large deformations. Appendix D.2.2 derives the corresponding constitutive equations. Appendices D.2.3 and D.2.4 detail the application to a simple example and to a complex one, respectively.

Appendix D.2.1. Elastic energy

At small deformations, the elastic response of an isotropic material can be expressed in terms of only two scalar coefficients, like in eq. (B.19). Conversely, at large elastic deformations, eq. (B.19) is only one possibility to quantify the elastic energy. There is no fundamental reason

to exclude other isotropic, convex functions of the deformation, and other higher order terms would be possible. Since $\text{tr} \varepsilon_1$ and $\text{dev} \varepsilon_1$ do not represent any longer the pure volume and pure shape contributions of the deformation ε_1 , eq. (B.19) is not technically convenient.

We now propose to define other quantities $\widehat{\text{tr}} \varepsilon_1$ and $\widehat{\text{dev}} \varepsilon_1$ which actually represent pure volume and shape contributions of the deformation ε_1 even at large deformations, as follows. They generalise $\text{tr} \varepsilon_1$ and $\text{dev} \varepsilon_1$ and can be similarly defined for any ε_k .

As derived in appendix D.1.3, a quantity relevant to describe large elastic deformation is the elongation $I + 2\varepsilon_1$, see eq. (D.17). The volume is proportional to the square root of its determinant $\det(I + 2\varepsilon_1)$ (see appendix A.2). We suggest to decompose $I + 2\varepsilon_1$ into the product of a scalar and a tensor of determinant unity

$$I + 2\varepsilon_1 = [\det(I + 2\varepsilon_1)]^{\frac{1}{d}} \frac{I + 2\varepsilon_1}{[\det(I + 2\varepsilon_1)]^{\frac{1}{d}}}. \quad (\text{D.26})$$

Since the decomposition is multiplicative, we take the logarithm of eq. (D.26) to write an equation that $\widehat{\text{tr}} \varepsilon_1$ and $\widehat{\text{dev}} \varepsilon_1$ should obey

$$\frac{1}{2} \log(I + 2\varepsilon_1) = \frac{\widehat{\text{tr}} \varepsilon_1}{d} I + \widehat{\text{dev}} \varepsilon_1, \quad (\text{D.27})$$

or equivalently

$$\varepsilon_1 = \frac{1}{2} \left[\exp \left(\frac{2\widehat{\text{tr}} \varepsilon_1}{d} I + 2\widehat{\text{dev}} \varepsilon_1 \right) - I \right]. \quad (\text{D.28})$$

For any symmetric, definite, positive tensor Q , there is an identity: $\log(\det Q) = \text{tr} \log Q$. As a consequence, we obtain the definitions of $\widehat{\text{tr}} \varepsilon_1$ and $\widehat{\text{dev}} \varepsilon_1$

$$\widehat{\text{tr}} \varepsilon_1 = \frac{1}{2} \text{tr} [\log(I + 2\varepsilon_1)], \quad (\text{D.29})$$

$$\widehat{\text{dev}} \varepsilon_1 = \frac{1}{2} \text{dev} [\log(I + 2\varepsilon_1)]. \quad (\text{D.30})$$

A natural possibility for the elastic energy, which tends toward eq. (B.19) in the limit of small deformations, reads

$$\mathcal{E} = G(\widehat{\text{dev}} \varepsilon_1)^2 + \frac{1}{2} K(\widehat{\text{tr}} \varepsilon_1)^2. \quad (\text{D.31})$$

The corresponding stress, which tends towards the elastic contribution to eq. (B.14) in the limit of small deformations, reads

$$\sigma = 2G\widehat{\text{dev}} \varepsilon_1 + K\widehat{\text{tr}} \varepsilon_1 I. \quad (\text{D.32})$$

Equation (D.31) is only an example of an isotropic, convex function of the deformation, and additional terms will generally be needed to describe the elasticity of any given material. The actual choice should be informed by relevant quantitative experimental measurements. In the incompressible limit, eqs. (D.31), (D.32) become

$$\widehat{\text{tr}} \varepsilon_1 = 0, \quad (\text{D.33})$$

$$\mathcal{E} = G(\widehat{\text{dev}} \varepsilon_1)^2, \quad (\text{D.34})$$

$$\text{dev} \sigma = 2G\widehat{\text{dev}} \varepsilon_1. \quad (\text{D.35})$$

Appendix D.2.2. Constitutive equations

The dissipation function is written with the symmetrised velocity gradient D and its effective counterpart D_1 (see appendix D.1.4); since they always correspond to small deformation increments $D dt$ and $D_1 dt$, \mathcal{D} is written using the usual traces and deviators, rather than with the large deformation versions. Indeed, the reader may check, using eqs. (D.7), (D.24), (D.29), (D.30) that

$$(\partial_t + \mathbf{v} \cdot \nabla) [\widehat{\text{tr}} \varepsilon] = \text{tr } D, \quad (\text{D.36})$$

$$(\partial_t + \mathbf{v} \cdot \nabla) [\widehat{\text{dev}} \varepsilon] = \text{dev } D, \quad (\text{D.37})$$

$$(\partial_t + \mathbf{v} \cdot \nabla) [\widehat{\text{tr}} \varepsilon_1] = \text{tr } D_1, \quad (\text{D.38})$$

$$(\partial_t + \mathbf{v} \cdot \nabla) [\widehat{\text{dev}} \varepsilon_1] = \text{dev } D_1. \quad (\text{D.39})$$

The differentiation rule of the energy and dissipation function given by eqs. (B.10)-(B.13) is now rewritten using D and D_1

$$\text{dev } \sigma = \frac{\partial \mathcal{D}}{\partial \text{dev } D} + \frac{\partial \mathcal{E}}{\partial \widehat{\text{dev}} \varepsilon}, \quad (\text{D.40})$$

$$\text{tr } \sigma = \frac{\partial \mathcal{D}}{\partial \text{tr } D} + \frac{\partial \mathcal{E}}{\partial \widehat{\text{tr}} \varepsilon}, \quad (\text{D.41})$$

$$0 = \frac{\partial \mathcal{D}}{\partial \text{dev } D_1} + \frac{\partial \mathcal{E}}{\partial \widehat{\text{dev}} \varepsilon_1}, \quad (\text{D.42})$$

$$0 = \frac{\partial \mathcal{D}}{\partial \text{tr } D_1} + \frac{\partial \mathcal{E}}{\partial \widehat{\text{tr}} \varepsilon_1}. \quad (\text{D.43})$$

Appendix D.2.3. Simple example

The large deformations ingredients can be implemented in the Maxwell viscoelastic liquid discussed in appendix B.2.

We rewrite the energy in terms of the large deformation versions of the trace and deviator of the deformations as in eq. (D.31), and the dissipation function as in eq. (B.20)

$$\mathcal{E} = G (\widehat{\text{dev}} \varepsilon_1)^2 + \frac{1}{2} K (\widehat{\text{tr}} \varepsilon_1)^2, \quad (\text{D.44})$$

$$\mathcal{D} = \eta (\text{dev } D - \text{dev } D_1)^2 + \frac{1}{2} \chi (\text{tr } D - \text{tr } D_1)^2. \quad (\text{D.45})$$

From eqs. (D.40)-(D.43), we obtain the equivalent of eqs. (B.15)-(B.18)

$$\text{tr } \sigma = \chi d (\text{tr } D - \text{tr } D_1), \quad (\text{D.46})$$

$$\text{dev } \sigma = 2\eta (\text{dev } D - \text{dev } D_1), \quad (\text{D.47})$$

$$0 = K d \widehat{\text{tr}} \varepsilon_1 + \chi d (\text{tr } D_1 - \text{tr } D), \quad (\text{D.48})$$

$$0 = 2G \widehat{\text{dev}} \varepsilon_1 + 2\eta (\text{dev } D_1 - \text{dev } D). \quad (\text{D.49})$$

Equations (D.36)-(D.39) and (D.46)-(D.49) are sufficient to describe the material evolution using a closed set of equations. Once the set of equations is solved, the deformations ε and ε_1 are recovered from the volume and shape components using eq. (D.28).

The modulus of $D\tau$ (called the ‘‘Weissenberg’’ number) is dimensionless: it is the ratio of the relaxation time to the typical time of the flow, and compares the material viscoelastic properties with the kinetics. As long as this number is moderately small, the situation remains similar to the small deformation case: the nonlinear problem is still well posed and efficient optimization algorithms could be used [91]. When this number becomes large, this property is lost in some cases, *e.g.* when the behavior of the material becomes close to an elastic body with large deformations in a complex geometry involving boundary layers.

Appendix D.2.4. Complex example

The energy and dissipation functions for tissue modelling represented by fig. 10 have been expressed explicitly in sect. 3.5.2 in the limit of small elastic deformations. At large elastic deformations, the corresponding expressions become

$$\mathcal{E} = G_1 (\widehat{\text{dev}} (\varepsilon_1))^2 + G_2 (\widehat{\text{dev}} (\varepsilon_2))^2, \quad (\text{D.50})$$

$$\begin{aligned} \mathcal{D} = & \eta_{\text{cyto}} (\text{dev } D_{\text{intra}} - \text{dev } D_1)^2 \\ & + \sigma_Y |\text{dev } D - \text{dev } D_{\text{intra}} - \text{dev } D_3 - \text{dev } D_{\text{ck}}| \\ & + \eta_3 (\text{dev } D_3)^2 + \frac{1}{2} \eta_{\text{sw}} (\text{tr } D_{\text{intra}} - r_{\text{sw}} + \text{tr } \dot{\varepsilon}_{\text{ck}})^2 \\ & + \frac{1}{2} \eta_{\text{apo}} (\text{tr } D - \text{tr } D_{\text{intra}} - \text{tr } D_{\text{ck}} + r_{\text{apo}})^2. \end{aligned} \quad (\text{D.51})$$

The resulting dynamic equations (not shown) are complemented by the kinematic equations for the deformations

$$\dot{\varepsilon} = D + \Omega \varepsilon - \varepsilon \Omega + D\varepsilon + \varepsilon D, \quad (\text{D.52})$$

$$\dot{\varepsilon}_1 = D_1 + \Omega \varepsilon_1 - \varepsilon_1 \Omega + D_1 \varepsilon_1 + \varepsilon_1 D_1, \quad (\text{D.53})$$

$$\begin{aligned} \dot{\varepsilon}_{\text{intra}} = & D_{\text{intra}} + \Omega \varepsilon_{\text{intra}} - \varepsilon_{\text{intra}} \Omega \\ & + D_{\text{intra}} \varepsilon_{\text{intra}} + \varepsilon_{\text{intra}} D_{\text{intra}}. \end{aligned} \quad (\text{D.54})$$

Equations (14), (22), (D.50)-(D.54) close the set of equations which determine the evolution of the tissue.

References

1. E.F. Keller, *Making sense of life: explaining biological development with models, metaphors, and machines* (Harvard University Press, 2002).
2. A. Huxley, R. Simmons, *Nature* **233**, 533 (1971).
3. Y. Fung, *Biomechanics: Mechanical Properties of Living Tissues* (Springer Verlag, 2010).
4. G. Forgacs, S.A. Newman, *Biological Physics of the Developing Embryo* (Cambridge University Press, 2005).
5. C.P. Heisenberg, Y. Bellaïche, *Cell* **153**, 948 (2013).
6. I.W. Hamley, *Introduction to Soft Matter. Polymers, Colloids, Amphiphiles and Liquid Crystals* (John Wiley and Sons, 2010).
7. M. Caruel, J.M. Allain, L. Truskinovsky, *Phys. Rev. Lett.* **110**, 248108 (2013).
8. G. Forgacs, R.A. Foty, Y. Shafir, M.S. Steinberg, *Biophys. J.* **74**, 2227 (1998).
9. J. Ranft, M. Basan, J. Elgeti, J.F. Joanny, J. Prost, F. Jülicher, *Proc. Natl. Acad. Sci. U.S.A.* **107**, 20863 (2010).

10. P. Marmottant, A. Mgharbel, J. Käfer, B. Audren, J.P. Rieu, J.C. Vial, B. van der Sanden, A.F.M. Marée, F. Graner, H. Delanoë-Ayari, *Proc. Natl. Acad. Sci. U.S.A.* **106**, 17271 (2009).
11. R. David, O. Luu, E.W. Damm, J.W.H. Wen, M. Nagel, R. Winklbauer, *Development* **141**, 1 (2014).
12. F. Montel, M. Delarue, J. Elgeti, L. Malaquin, M. Basan, T. Risler, B. Cabane, D. Vignjevic, J. Prost, G. Cappelletti *et al.*, *Phys. Rev. Lett.* **107**, 188102 (2011).
13. L. LeGoff, H. Rouault, T. Lecuit, *Development* **140**, 4051 (2013).
14. P. Fernandez, M. Maier, M. Lindauer, C. Kuffer, Z. Storchova, A. Bausch, *PLoS One* **6**, e28965 (2011).
15. L. Wolpert, J. Smith, T. Jessell, P. Lawrence, E. Robertson, E. Meyerowitz, *Principles of Development* (Oxford University Press, 2006).
16. A. McMahon, W. Supatto, S.E. Fraser, A. Stathopoulos, *Science* **322**, 1546 (2008).
17. P.J. Keller, A.D. Schmidt, J. Wittbrodt, E.H.K. Stelzer, *Science* **322**, 1065 (2008).
18. N. Olivier, M.A. Luengo-Oroz, L. Duloquin, E. Faure, T. Savy, I. Veilleux, X. Solinas, D. Débarre, P. Bourguine, A. Santos *et al.*, *Science* **329**, 967 (2010).
19. J. Moosmann, A. Ershov, V. Altapova, T. Baumbach, M.S. Prasad, C. LaBonne, X. Xiao, J. Kashef, R. Hofmann, *Nature* **497**, 374 (2013).
20. U. Krzic, S. Gunther, T.E. Saunders, S.J. Streichan, L. Hufnagel, *Nat. Methods* **9**, 730 (2012).
21. C. Bertet, L. Sulak, T. Lecuit, *Nature* **429**, 667 (2004).
22. B. Aigouy, R. Farhadifar, D.B. Staple, A. Sagner, J.C. Röper, F. Jülicher, S. Eaton, *Cell* **142**, 773 (2010).
23. F. Bosveld, I. Bonnet, B. Guirao, S. Tlili, Z. Wang, A. Petitalot, R. Marchand, P.L. Bardet, P. Marcq, F. Graner *et al.*, *Science* **336**, 724 (2012).
24. O. Wartlick, A. Kicheva, M. González-Gaitán, *Cold Spring Harbor Persp. Biol.* **1**, a001255 (2009).
25. M.S. Hutson, Y. Tokutake, M.S. Chang, J.W. Bloor, S. Venakides, D.P. Kiehart, G.S. Edwards, *Science* **300**, 145 (2003).
26. I. Bonnet, P. Marcq, F. Bosveld, L. Fetler, Y. Bellaïche, F. Graner, *J. R. Soc. Interface* **9**, 2614 (2012).
27. G.W. Brodland, V. Conte, P.G. Cranston, J. Veldhuis, S. Narasimhan, M.S. Hutson, A. Jacinto, F. Ulrich, B. Baum, M. Miodownik, *Proc. Natl. Acad. Sci. U.S.A.* **107**, 22111 (2010).
28. K.K. Chiou, L. Hufnagel, B.I. Shraiman, *PLoS Comput. Biol.* **8**, e1002512 (2012).
29. S. Ishihara, K. Sugimura, *J. theor. Biol.* **313**, 201 (2012).
30. K. Sugimura, S. Ishihara, *Development* **140**, 4091 (2013).
31. J.L. Maître, H. Berthoumieux, S.F.G. Krens, G. Salbreux, F. Jülicher, E. Paluch, C.P. Heisenberg, *Science* **338**, 253 (2012).
32. O. Campàs, T. Mammoto, S. Hasso, R.A. Sperling, D. O'Connell, A.G. Bischof, R. Maas, D.A. Weitz, L. Mahadevan, D.E. Ingber, *Nat. Methods* **11**, 183 (2014).
33. N. Borghi, M. Sorokina, O.G. Shcherbakova, W.I. Weis, B.L. Pruitt, W.J. Nelson, A.R. Dunn, *Proc. Natl. Acad. Sci. U.S.A.* **109**, 12568 (2009).
34. X. Trepât, M.R. Wasserman, T.E. Angelini, E. Millet, D.A. Weitz, J.P. Butler, J.J. Fredberg, *Nat. Phys.* **5**, 426 (2009).
35. T.E. Angelini, E. Hannezo, X. Trepât, J.J. Fredberg, D.A. Weitz, *Phys. Rev. Lett.* **104**, 168104 (2010).
36. A. Saez, E. Anon, M. Ghibaudo, O. du Roure, J.-M. di Meglio, P. Hersen, P. Silberzan, A. Buguin, B. Ladoux, *J. Phys.: Condens. Matter* **22**, 194119 (2010).
37. M. Reffay, L. Petitjean, S. Coscoy, E. Grasland-Mongrain, F. Amblard, A. Buguin, P. Silberzan, *Biophys. J.* **100**, 2566 (2011).
38. X. Serra-Picamal, V. Conte, R. Vincent, E. Anon, D.T. Tambe, E. Bazellieres, J.P. Butler, J.J. Fredberg, X. Trepât, *Nat. Phys.* **8**, 628 (2012).
39. A.R. Harris, L. Peter, J. Bellis, B. Baum, A.J. Kabla, G.T. Charras, *Proc. Natl. Acad. Sci. U.S.A.* **109**, 16449 (2012).
40. K. Doxzen, S.R.K. Vedula, M.C. Leong, H. Hirata, N.S. Gov, A.J. Kabla, B. Ladoux, C.T. Lim, *Integr. Biol.* **5**, 1026 (2013).
41. O. Cochet-Escartin, J. Ranft, P. Silberzan, P. Marcq, *Biophys. J.* **106**, 65 (2014).
42. D. Gonzalez-Rodriguez, K. Guevorkian, S. Douezan, F. Brochard-Wyart, *Science* **338**, 910 (2012).
43. K. Alessandri, B.R. Sarangi, V.V. Gurchenkov, B. Sinha, T.R. Kieling, L. Fetler, F. Rico, S. Scheuring, C. Lamaze, A. Simon *et al.*, *Proc. Natl. Acad. Sci. U.S.A.* **110**, 14843 (2013).
44. A. Mgharbel, H. Delanoë-Ayari, J.P. Rieu, *HFSP J.* **3**, 213 (2009).
45. T.V. Stirbat, S. Tlili, T. Houver, C. Barentin, J.P. Rieu, H. Delanoë-Ayari, *Eur. Phys. J. E* **36**, 84 (2013).
46. R. Tomer, K. Khairy, F. Amat, P.J. Keller, *Nat. Methods* **9**, 755 (2012).
47. T. Nagai, H. Honda, *Philos. Mag. B* **81**, 699 (2001).
48. A.F.M. Marée, V.A. Grieneisen, P. Hogeweg, *The Cellular Potts Model and biophysical properties of cells, tissues and morphogenesis*, in *Single Cell-Based Models in Biology and Medicine*, edited by A.R.A. Anderson, M. Chaplain, K.A. Rejniak (Birkhäuser Verlag, Basel, 2007) pp. 107–136.
49. D. Drasdo, S. Hoehme, M. Block, *J. Stat. Phys.* **128**, 287 (2007).
50. J. Solon, A. Kaya-Çopur, J. Colombelli, D. Brunner, *Cell* **137**, 1331 (2009).
51. B. Vasiev, A. Balter, M. Chaplain, J.A. Glazier, C.J. Weijer, *PLoS One* **5**, e10571 (2010).
52. G.W. Brodland, X. Chen, P. Lee, M. Marsden, *HFSP J.* **4**, 142 (2010).
53. A.J. Kabla, *J. R. Soc. Interface* **9**, 3268 (2012).
54. M.A. Wyczałkowski, Z. Chen, B.A. Filas, V.D. Varner, L.A. Taber, *Birth Defects Res. C* **96**, 132 (2012).
55. M. Basan, J. Elgeti, E. Hannezo, W.J. Rappel, H. Levine, *Proc. Natl. Acad. Sci. U.S.A.* **110**, 2452 (2013).
56. N. Sepúlveda, L. Petitjean, O. Cochet, E. Grasland-Mongrain, P. Silberzan, V. Hakim, *PLoS Comput. Biol.* **9**, e1002944 (2013).
57. Y. Li, H. Naveed, S. Kachalo, L.X. Xu, J. Liang, *PLoS One* **9**, e86725 (2014).
58. J. Ortega, *Plant Physiol.* **79**, 318 (1985).
59. D.P. Pioletti, L.R. Rakotomanana, *Eur. J. Mech. A* **19**, 749 (2000).
60. P. Nardinocchi, L. Teresi, *J. Elast.* **88**, 27 (2007).
61. M. Basan, T. Risler, J.F. Joanny, X. Sastre-Garau, J. Prost, *HFSP J.* **3**, 265 (2009).
62. M. Basan, J.F. Joanny, J. Prost, T. Risler, *Phys. Rev. Lett.* **106**, 158101 (2011).
63. K. Guevorkian, M.J. Colbert, M. Durth, S. Dufour, F. Brochard-Wyart, *Phys. Rev. Lett.* **104**, 218101 (2010).

64. L. Preziosi, D. Ambrosi, C. Verdier, J. theor. Biol. **262**, 35 (2010).
65. P. Lee, C.W. Wolgemuth, PLoS Comput. Biol. **7**, e1002007 (2011).
66. M.H. Köpf, L.M. Pismen, Soft Matter **9**, 3727 (2012).
67. E.E. Kuchen, S. Fox, P. Barbier de Reuille, R. Kennaway, S. Bensmihen, J. Avondo, G.M. Calder, P. Southam, S. Robinson, A. Bangham *et al.*, Science **335**, 1092 (2012).
68. F. Graner, B. Dollet, C. Raufaste, P. Marmottant, Eur. Phys. J. E **25**, 349 (2008).
69. S. Bénito, C.-H. Bruneau, T. Colin, C. Gay, F. Molino, Eur. Phys. J. E **25**, 225 (2008).
70. S. Bénito, F. Molino, C.-H. Bruneau, T. Colin, C. Gay, Eur. Phys. J. E **35**, 1 (2012).
71. I. Cheddadi, P. Saramito, B. Dollet, C. Raufaste, F. Graner, Eur. Phys. J. E **34**, 1 (2011).
72. I. Cantat, S. Cohen-Addad, F. Elias, F. Graner, R. Höhler, O. Pitois, F. Rouyer, A. Saint-Jalmes, *Foams: structure and dynamics*, edited by S.J. Cox (Oxford University Press, 2013).
73. J.G. Oldroyd, Proc. Roy. Soc. London A **200**, 523 (1950).
74. P. Chaikin, T. Lubensky, *Principles of condensed matter physics* (Cambridge University Press, 1995).
75. P.C. Martin, O. Parodi, P.S. Pershan, Phys. Rev. A **6**, 2401 (1972).
76. P.G. de Gennes, J. Prost, *The Physics of Liquid Crystals*, 2nd ed. (Oxford University Press, 1993).
77. J. Toner, Y. Tu, S. Ramaswamy, Ann. Phys. **318**, 170 (2005).
78. E. Bertin, M. Droz, G. Grégoire, J. Phys. A **42**, 445001 (2009).
79. F. Jülicher, K. Kruse, J. Prost, J.F. Joanny, Phys. Rep. **449**, 3 (2007).
80. M.C. Marchetti, J.F. Joanny, S. Ramaswamy, T.B. Liverpool, J. Prost, M. Rao, R.A. Simha, Rev. Mod. Phys. **85**, 1143 (2013).
81. S.R. de Groot, P. Mazur, *Non-Equilibrium Thermodynamics* (Dover Publications, 1985).
82. L. Landau, E. Lifshitz, *Statistical Physics* (Butterworth-Heinemann, 1975).
83. B. Halphen, Q. Nguyen, J. Méc. **14**, 39 (1975).
84. G. Maugin, *The thermomechanics of plasticity and fracture* (Cambridge, 1992).
85. P. Saramito, *Méthodes numériques en fluides complexes: théorie et algorithmes* (CNRS-CCSD, 2012), <http://cel.archives-ouvertes.fr/cel-00673816>.
86. G.T. Houlsby, *Dissipation rate functions, Pseudopotentials, Potentials and Yield Surfaces*, in *Beyond the Second Law* (Springer-Verlag, 2014) pp. 73–95.
87. P. Saramito, J. Non-Newt. Fluid Mech. **145**, 1 (2007).
88. P. Saramito, J. Non-Newt. Fluid Mech. **158**, 154 (2009).
89. P.L. Tallec, *Numerical analysis of viscoelastic problems* (Masson, 1990).
90. I. Cheddadi, P. Saramito, F. Graner, J. Rheol. **56**, 213 (2012).
91. I. Cheddadi, P. Saramito, J. Non-Newtonian Fluid Mech. **202**, 13 (2013).
92. L.A. Taber, *Nonlinear Theory of Elasticity: Applications in Biomechanics* (World Scientific, 2004).
93. S. Bénito, Ph.D. thesis, Université Bordeaux 1, Bordeaux, France (2009), <http://tel.archives-ouvertes.fr/tel-00525106/fr/>.
94. I. Cheddadi, Ph.D. thesis, Université Joseph-Fourier - Grenoble I, Grenoble, France (2010), <http://tel.archives-ouvertes.fr/tel-00497436/>.
95. E.M. Schoetz, M. Lanio, J.A. Talbot, M.L. Manning, J. R. Soc. Interface **10**, 20130726 (2013).
96. K.D. Nnetu, M. Knorr, J. Käs, M. Zink, New J. Phys. **14**, 115012 (2013).
97. D. Bi, J.H. Lopez, J.M. Schwarz, M.L. Manning, Soft Matter **10**, 1885 (2014).
98. N. Roquet, P. Saramito, Comput. Appl. Meth. Mech. Engrg. **192**, 3317 (2003).
99. A. Puliafito, L. Hufnagel, P. Neveu, S. Streichan, A. Sigal, D.K. Fygenon, B.I. Shraiman, Proc. Natl. Acad. Sci. U.S.A. **109**, 739 (2012).
100. T. Bittig, O. Wartlick, A. Kicheva, M. González-Gaitán, F. Jülicher, New J. Phys. **11**, 063001 (2008).
101. T. Bittig, O. Wartlick, M. González-Gaitán, F. Jülicher, Eur. Phys. J. E **30**, 93 (2009).
102. T. McMahon, *Muscles, Reflexes, and Locomotion* (Princeton University Press, Princeton, 1984).
103. K. Kruse, J.F. Joanny, F. Jülicher, J. Prost, K. Sekimoto, Phys. Rev. Lett. **92**, 078101 (2004).
104. J. Étienne, J. Fouchard, D. Mitrossilis, N. Bufi, P. Durand-Smet, A. Asnacios, Proc. Natl. Acad. Sci. U.S.A. **112**, 2740 (2015).
105. A.M. Sonnet, E.G. Virga, Phys. Rev. E **64**, 031705 (2001).
106. A.M. Sonnet, P.L. Maffettone, E.G. Virga, J. Non-Newtonian Fluid Mech. **119**, 51 (2004).
107. A. Desmaison, C. Frongia, K. Grenier, B. Ducommun, V. Lobjois, PLoS One **8**, e80447 (2013).
108. P. Pereira, M.P. Valignat, J. Bico, O. Théodoly, Biomecrofluidics **7**, 024111 (2013).
109. T.V. Stirbat, A. Mgharbel, S. Bodennec, K. Ferri, H.C. Mertani, J.P. Rieu, H. Delanoë-Ayari, PLoS One **8**, e52554 (2013).
110. C. Blanch-Mercader, J. Casademunt, J.F. Joanny, Eur. Phys. J. E **37**, 41 (2014).
111. G.B. Blanchard, A.J. Kabla, N.L. Schultz, L.C. Butler, B. Sanson, N. Gorfinkiel, L. Mahadevan, R.J. Adams, Nat. Methods **6**, 458 (2009).
112. L.C. Butler, G.B. Blanchard, A.J. Kabla, N.J. Lawrence, D.P. Welchman, L. Mahadevan, R.J. Adams, B. Sanson, Nat. Cell Biol. **11**, 859 (2006).
113. J.S. Bois, F. Jülicher, S.W. Grill, Phys. Rev. Lett. **106**, 028103 (2011).
114. P. Marcq, Eur. Phys. J. E **37**, 29 (2014).
115. G. Duclos, S. Garcia, H.G. Yevick, P. Silberzan, Soft Matter **10**, 2346 (2014).
116. D.D. Joseph, *Fluid dynamics of viscoelastic liquids* (Springer, 1990).
117. P. Oswald, *Rheophysics: The Deformation and Flow of Matter* (Cambridge University Press, 2009).
118. E. Rouhaud, B. Panicaud, R. Kerner, Comput. Mater. Sci. **77**, 120 (2013).

The authors represent a collaboration from different fields that complement each other for the topic of the present article: biology, biophysics, theoretical physics and applied mathematics. Some of the authors are members of the Academy of Bradylogists. They declare that scientific work takes time. It takes time to think differently and sometimes it takes time to be wrong. They believe that collaboration is more fecund than competition, and that only time can state about the quality of a research work, as opposed to the excessive use of labels, fast evaluations and judgments.